Journal Pre-proof

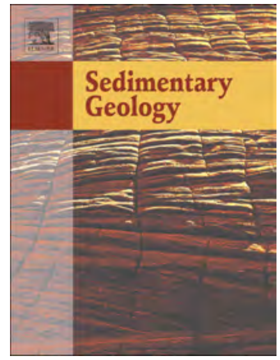

Factors governing travertine deposition in fluvial systems: The Bagni San Filippo (central Italy) case study

Lianchao LUO, Enrico CAPEZZUOLI, Orlando VASELLI, Huaguo WEN, Marta LAZZARONI, Zhipeng LU, Federica MELONI, Sándor KELE

PII: S0037-0738(21)00175-5

DOI: https://doi.org/10.1016/j.sedgeo.2021.106023

Reference: SEDGEO 106023

To appear in: *Sedimentary Geology*

Received date: 14 September 2021

Revised date: 15 October 2021

Accepted date: 15 October 2021

Please cite this article as: L. LUO, E. CAPEZZUOLI, O. VASELLI, et al., Factors governing travertine deposition in fluvial systems: The Bagni San Filippo (central Italy) case study, *Sedimentary Geology* (2021), https://doi.org/10.1016/j.sedgeo.2021.106023

Factors governing travertine deposition in fluvial systems: The Bagni San Filippo (central Italy) case study

Lianchao LUO [1,*], Enrico CAPEZZUOLI [1], Orlando VASELLI [1,2], Huaguo WEN [3,4], Marta LAZZARONI [1,2], Zhipeng LU [4], Federica MELONI [5], Sándor KELE [6]

[1] Department of Earth Sciences, University of Florence, Firenze 50121, Italy

[2] CNR-IGG Institute of Geosciences and Earth Resources, Florence 50121, Italy

[3] State Key Laboratory of Oil and Gas Reservoir Geology and Exploitation (Chengdu University of Technology), Chengdu 610059, China

[4] Institute of Sedimentary Geology, Chengdu University of Technology, Chengdu 610059, China

[5] INSTM - National Interuniversity Consortium of Materials Science and Technology, Via Giusti 9, Florence 50121, Italy

[6] Institute for Geological and Geochemical Research, Research Centre for Astronomy and Earth Sciences, H-1112 Budapest, Hungary

** Corresponding author: lianchao.luo@unifi.it (Luo L.)*

Abstract

Although fossil fluvial travertines have been described, factors controlling their formation are poorly understood because of the paucity of their modern counterparts. To disclose processes affecting their deposition, a modern fluvial travertine system at Bagni San Filippo (Siena, central Italy) was studied here and compared with other cases. The studied travertines occur in a valley with an ephemeral stream, but continuous water influx from hot springs on the hillside causes part of the stream become perennial. Four sub-environments were recognized: slopes, waterfalls, pools, and channels. The first two are mainly composed of laminated crystalline crust-boundstone. In contrast, pools are mainly covered by lime mud and some post-flood travertine-encrusted breccia, while channels commonly display abundant travertine-encrusted breccia. Many erosional features/products were also found and are largely the result of episodic erosional events triggered by heavy rainfalls and accompanied floods. The predominant erosional processes might include abrasion and plucking. Based on environment distribution, stream bed morphology, and erosional distinctions, the fluvial system was distinguished into slope-pool-waterfall and channel-pool-waterfall subsystems. Such system differentiation is attributed to the original stream bed difference: wide beds promoted the development of slopes, while narrow beds encouraged travertine erosion and subsequent gravel accumulation during flood events, favoring the formation of channels. The comparison shows that fluvial travertine deposition largely occurs within “existing” rivers. The relative contribution of spring water to original river water controls the deposit composition (the higher contribution ratios, the more abundant carbonate/travertine facies). Furthermore, erosion might be common and unavoidable because the reported fluvial travertines were all formed in non-arid regions. These findings suggest that fluvial travertine deposition is influenced by topography, hot spring contribution, original river bed geometry, and fluvial erosion, and might aid in the interpretation of ancient fluvial travertine systems. Additionally, downstream fluvial travertine systems might show similar characteristics to fluvial tufa, but their formation is clearly hot spring influenced, indicating the importance of analyzing facies distribution and $\delta^{13}C$-$\delta^{18}O$ signatures in fluvial carbonate studies.

Keywords: fluvial travertine, C-O stable isotopes, hot spring, erosion, central Italy

1 Introduction

Terrestrial carbonate deposits can be commonly found around cold springs (i.e. tufa or meteogene travertine) and warm-hot springs (i.e. travertine or thermogene travertine) (e.g. Pentecost and Viles, 1994; Ford and Pedley, 1996; Pentecost, 2005; Jones and Renaut, 2010; Capezzuoli et al., 2014). With respect to these spring-constructed carbonates, multiple depositional models have been built based on their morphologies, lithofacies and facies associations: tufa depositional models are generally divided into perched springline model, fluvial model, paludal model, lacustrine model, and cascade model, while the classification of travertine depositional models is much different, encompassing fissure ridge model, terraces and range front sheet model, slope model, depression model, and mound model (e.g. Pedley, 1990; Ford and Pedley, 1996; Pedley, 2009; Capezzuoli et al., 2014; Della Porta, 2015; Toker et al., 2015; Mancini et al., 2019; Brogi et al., 2021; Kandemir et al., 2021). All the classifications considered "rivers/streams" as potential depositional areas for spring-constructed carbonates, but only for tufa (e.g. Drysdale and Gillieson, 1997; Arenas et al., 2010; Gradziński, 2010; Vázquez-Urbez et al., 2012; Arenas et al., 2015; Bastianini et al., 2019).

Özkul et al. (2014), however, observed some elongated travertine build-ups of about several kilometers long along an ephemeral stream valley in Aksaz, Turkey, and established a fluvial model composed of pools, waterfalls, and slopes to interpret the unusual distribution and development of these travertines. Additionally, erosion surfaces and clastic deposits (conglomerates and sandstones) were also recorded in this system and were speculated as results of flooding after occasional heavy rains (Özkul et al., 2014). An analogous fossil fluvial travertine system was also found in Azuaje, Spain, but intraformational clastic deposits were not documented (Rodríguez-Berriguete et al., 2012; Rodríguez-Berriguete and Alonso-Zarza, 2019). Instead, erosive discontinuities within the fluvial travertines at several scales are reported (Rodríguez-Berriguete and Alonso-Zarza, 2019). One modern fluvial travertine system is documented in Ngol, Cameroon and allochthonous detrital gravels and sands coated by calcite were also confirmed within the pools along the stream (Bisse et al., 2018). These indicate that fluvial environments are able to deposit travertines and erosion might be universal in fluvial systems. However, the first two reported fluvial travertine systems are fossil deposits partly cropped out at the surface and the locations and water chemistry of their headsprings are unknown (Rodríguez-Berriguete et al., 2012; Özkul et al., 2014; Rodríguez-Berriguete and Alonso-Zarza, 2019), whereas the last case focuses on the depositional environment and geochemistry of travertines (Bisse et al., 2018). These make it difficult to disclose the processes associated with their deposition and possible erosion.

At Bagni San Filippo (central Italy), hot springs produced extensive travertines along faults (Fig. 1A, B). Even though most of them are non-active at present, modern hot springs still exist along a valley near the village. Thermal water from these springs continuously inputs into the valley, forming a north-flowing "hot-water stream" (i.e. Fosso Bianco, meaning "White Creek"), but temporary (pure) stream water and rainwater also serve as episodic supplies of the stream (Fig. 1C). The combination of these fluids generates lots of travertine deposits with conspicuous erosional discontinuities and siliciclastic sediments within the river bed, forming a modern travertine-depositing fluvial system and providing a good example for fluvial travertine studies. In this study, the hydrochemical, sedimentological, petrological, and stable carbon-oxygen isotope features of this system were thus examined. Accordingly, this study analyzed the factors affecting deposition and erosion of the studied fluvial travertines and compared them with the reported fossil counterparts to ascertain the context forming fluvial travertines. The knowledge might aid in the sedimentological interpretation of fossil fluvial travertines and might be conducive to the paleoenvironmental reconstruction of ancient fluvial travertine systems.

2 Geological setting

Bagni San Filippo (42°55'43.76''N, 11°42'12.51''-E) is located in southeastern Tuscany (central Italy), about 54 km south of Siena (Fig. 1A). Around Bagni San Filippo, Ligurian Units (Jurassic to Eocene ophiolites, shales, sandstones, calcarenites and marls) and Neogene-Quaternary sedimentary deposits mainly consisting of continental and marine sediments are widely distributed, while Mesozoic carbonate rocks with minor evaporites and Cenozoic pelagic-turbiditic deposits (i.e. Tuscan Nappe) crop out to the west (Fig. 1B) (e.g. Brogi, 2004; Brogi and Fabbrini, 2009; Brogi et al., 2015; Marroni et al., 2015). Travertine build-ups, like fissure ridges, mounds, and slopes (Capezzuoli et al., 2011; Capezzuoli et al., 2014; Gradziński et al., 2018; Della Porta et al., 2021) are patchily distributed at western Bagni San Filippo (Fig. 1B). The two biggest travertine bodies are located in the eastward tip zone of a NE-SW strike-slip fault and its associated E-W secondary faults in the surrounding of the village (Brogi et al., 2015). The fossil, higher one which is up to 40 m thick and was probably formed in Late Pleistocene (Minissale, 2004) is characterized by several abandoned quarries showing its internal architecture of ridges/mound forming terraced/smooth slopes and tabular to fan-slope deposits that distally interacted with fluvial system (Rondinaio Creek). The active, topographically lower, travertine body shows similar depositional characteristics, with mound/fissure ridge in the higher portion and interaction with fluvial system (Bianco Creek) in its distal, eastern part. Thermal waters episodically issue from the higher portion, while dominantly gush out in the lower portion from springs located at the base of the travertine body or from anthropic pipelines (White Whale spring) (Fig. 1C).

The studied area experiences a sub-Mediterranean climate with contrasting air temperature variations. Average air temperatures at Abbadia San Salvatore (ca. 5.5 km away from Bagni San Filippo, Fig. 1A) in summers (June to August) between 2010 and 2020 range from 15 to 35 °C, different from the cold winter (December to February, −5 to 10 °C) (Fig. 2A, B). Annual rainfall amounts are commonly in excess of 1200 mm, but seasonal changes in precipitation are not apparent (Fig. 2A, B). Daily precipitation is basically lower than 50 mm, but can exceed 100 mm sometimes and is generally accompanied by flood events, like the November 2012 (Pattelli et al., 2014) and July 2019 flood events (Fig. 2). Water table information of the studied stream, which is a north-flowing tributary of Formone Creek (Fig. 1B) entering the Orcia River, is absent. However, data from the Monte Amiata Scalo stream gauging station (Fig. 1B) reflect the frequent water table peaks of the Orcia River from November to April and the low and stable water level between May to October (Fig. 2B).

Surface hydrothermal activity is still active nowadays at Bagni San Filippo, producing several springs near the village and their associated travertine deposits, especially in the west bank of the studied stream (Fig. 1B, C). Early reports (e.g. Bencini et al., 1977; Duchi et al., 1987; Minissale, 2004; Frondini et al., 2008; Chiodini et al., 2020) show that these springs are mostly hot (mostly between 35 and 50 °C) and near neutral springs enriched in Ca^{2+}, Mg^{2+}, HCO_3^-, and SO_4^{2-}. In addition, waters from these hot springs are generally considered to be mixtures of condensates of hydrothermal steam, deep-originated CO_2 and recharged rainwaters (Chiodini et al., 2020). Gas emissions are much common in most of the hot springs at Bagni San Filippo. The most predominant gas component is CO_2 (typically > 950 mmol/mol), while few N_2, H_2S, CH_4, O_2, H_2, He, Ar, and CO were also confirmed (Duchi et al., 1992; Tassi et al., 2012; Chiodini et al., 2020). Early reports about the modern travertine deposits at Bagni San Filippo showed that they were mainly composed of calcite, while some aragonite and trace gypsum were also observed (Kele et al., 2015; Kluge et al., 2018; Della Porta et al., 2021).

3 Materials and methods

Water temperature, pH, and total dissolved solids (TDS), were measured in the field using a Crison MM40+ portable instrumentation. In February 2021, acidified filtered water samples (for cation analysis) and non-acidified samples (for anion and NH_4) were collected from ten sites along the studied stream (Fig. 1C). Two of them (Un1 and White Whale) were pure hot spring water, while F1 represented pure stream water without any input of spring water. The rests (F2 to F8) were stream water samples mixed with hot spring water. The HCO_3^{-} and CO_3^{2-} contents were determined by titration using a 645 Multi Dosimat titrimeter (Metrohm) within 18h from the sampling: two milliliters of spring water were prepared in a breaker and two drops of phenolphthalein indicator and some 0.01mol/L hydrochloric acid were then dripped into the breaker to check the presence of CO_3^{2-}, and the concentrations of HCO_3^{-} and CO_3^{2-}, respectively. In our samples, no CO_3^{2-} was detected during the titration. Ammonia was analyzed by a portable datalogging molecular spectrophotometer (HACH DR/2010). Determination of other cations (Na^{+}, K^{+}, Ca^{2+}, Mg^{2+}) and anions (F^{-}, Cl^{-}, Br^{-}, SO_4^{2-}, NO_3^{-}) were performed by an 861 Advanced Compact IC and a 761 Compact IC (Metrohm), respectively. All the above analyses were carried out at the University of Florence.

PHREEQC (version 3) was employed to compute the saturation indexes of calcite (SI_C) and CO_2 partial pressures (log P_{CO2}) in the spring water, based on the WATEQ4F database (Parkhurst and Appelo, 2013). Besides, a mixing model between the local "White Whale" hot spring water and rainwater (T = 20 °C) from Rufeno Mt. (ca. 20 km away from the studied area, Fig. 1A) (Mosello et al., 2002) was constructed to evaluate the influence of rainwater input on water chemistry, and calcite precipitation and dissolution potentials. The process-based calcite growth model from Wolthers et al. (2012, their Eq. 34), which was applied by evaluating calcite precipitation in tufa systems (Bastianini et al., 2019), was adopted to determine the probable travertine depositional rate (R) in each site along the stream using the measured water temperature, ionic strength, CO_3^{2-} and Ca^{2+} activities, and calcite saturation ratios (i.e. $\Omega^{0.5} = 10^{0.5*SI}$) obtained from PHREEQC.

Fossil and modern travertine deposits in the studied stream were collected and dried before the preparation of thin sections. Microscopic and mineralogical features of travertine deposits were carefully investigated in sixteen thin sections at the University of Florence (Italy). Eight small fractured specimens were gold coated and then analyzed by a Quanta 250 FEG scanning Electron Microscope (SEM) coupled with an energy dispersive X-ray spectrometer at the Chengdu University of Technology (China) to examine the fabric characteristics. Stable carbon and oxygen isotope compositions of eleven representative travertine samples (fossil and modern) were determined using an automated carbonate preparation device (Gasbench II) and a Thermo Fisher Scientific Delta Plus XP continuous flow mass spectrometer at the Institute for Geological and Geochemical Research, Budapest (Hungary). Carbonate powders were reacted with 100% phosphoric acid at 70 °C. Standardization was conducted using laboratory calcite standards calibrated against the NBS−19 standard. The carbon and oxygen isotopic compositions are expressed in the conventional delta notation against the international standard V−PDB (for $\delta^{13}C$ and $\delta^{18}O$). One-sigma reproducibility for both C and O isotope analyses is better than ± 0.1‰.

4 Results

4.1 General description and zonation

The studied system (Fosso Bianco, meaning “White Creek”) is a small north-flowing stream with a length of about two kilometers and finally joins a larger tributary (Rondinaio Creek) of the Orcia River (Figs. 1B, C, 3). It is a typical ephemeral stream in central Italy, but permanent flow exists in the reach (ca. 550 m long) near the village of Bagni San Filippo due to the continuous water supply of several hot springs in the left stream bank, forming a modern hot spring controlled stream system. However, many of the hot springs are low in discharge, while there are three important spring-water adding points along the stream. Water from the first point (i.e. F2 in Fig. 1C) mainly derived from groundwater seeping (Fig. 3C). The second spring water input point is located near F3 (Fig. 1C), where thermal water (ca. 40 °C) is primarily discharged from Un1 and several nearby small hot springs (Fig. 3D). The last, but also the most significant, spring water contribution site is at “White Whale” (Fig. 3F, G). Long-term hot spring activity build an amazing platform-like travertine build-up and the significant import of thermal spring water and associated travertine deposition directly cause the whiting of the stream and generate numerous travertines before the confluence (Fig. 3F).

Based on the deposit composition, spring water contribution, and stream widths, the studied stream can be divided into four zones (A, B, C, and D) from upstream to downstream (Fig. 1C). Zone A is the stream reach without the impact of hot springs. This zone is often less than 5 m wide and lacks moder travertine deposition (Fig. 3A, B). Only siliciclastic gravels (mainly cobbles to boulders) and few travertine clasts exist in the stream bed. Infiltration is present in Zone A (Fig. 3A) and stream water discharge is variable in different seasons. Stream water is generally present in the cold wet winter (Fig. 3A), but disappears in the hot dry summer (Fig. 3B). Deposits and stream width of Zone B are similar to those of Zone A, but permanent flow is present in Zone B because of the visible input of thermal spring water. Zone C is characterized by a wide stream bed (typically ≥ 10 m) and receives more spring waters from small hot springs in the left-hand side bank with respect to those characterizing Zone B, especially from Un1 and its nearby springs (Fig. 3D, E). In Zone C, modern travertines can be observed in some places, like downstream slopes and waterfalls. This zone is heavily covered by fossil travertines, but is still partly filled by some siliciclastic gravels. Zone D represents an area where a large amount of waters sourced from thermal springs near White Whale exists and produces many modern carbonate deposits (Fig. 3F, G). Different from Zone C, the stream bed becomes narrow (only several meters in width) in Zone D. Water in Zone D would input another gravel-floored river and mix with the river water (Fig. 1C). Travertine deposition after the river confluence point becomes weaker, especially in winter (Fig. 3H), but is still non-negligible in summer (Fig. 3I).

4.2 Environments and lithofacies

The field observations recognized four basic sub-environments according to their geometry and facies, including waterfalls (e.g. Fig. 3E, G), pools (e.g. Fig. 3G), slopes (e.g. Fig. 3D), and channels (e.g. Fig. 3C) and eight lithofacies: laminated crystalline crust-boundstone, lime mud, microbial boundstone, phytoherm boundstone, phytoclast rudstone, travertine-encrusted breccia, mixed siliciclastic-carbonate sands-gravels, and sand-gravel sediment (Table 1, Figs. 4-7). Waterfalls and pools are generally laterally connected and occur in both Zone C and Zone D. Waterfalls mainly formed of laminated crystalline crust-boundstone (Figs. 4A, C, 5A) are up to several meters, but most of them are small stepped build-ups (morphologically similar to terraced slopes) and closely connected by small pools (e.g. Fig. 3E). Pools are low-energy environments with nearly stagnant water and are often several meters in diameter and less than one meter in depth. Deposits filling the pools are dominantly made up of lime mud and travertine-encrusted breccia. Slightly inclined slopes primarily composed of laminated crystalline crust-boundstone is the predominant element in Zone C and can extend more than ten meters in width and tens of meters in length (Fig. 3D). In contrast, channels, prevailing in Zone D, are much narrow (generally ≤ 5 meters) and are filled by travertine-encrusted gravels/phytoclast and a few travertine clasts (Figs. 4D, 5D).

The most prevailing facies is laminated crystalline crust-boundstone mainly developing in waterfalls and slopes (Figs. 4A, C, 5A). The newly formed laminated crystalline crust-boundstone is characterized by the striking alternation of white and yellow laminae (Fig. 4A, C), but even though lamination is still notable for samples from the fossil travertines, color variation disappears (Fig. 5A). For the modern samples, the white laminae can reach up to about 1 cm thick (generally ranging from 0.2 to 0.5 cm), significantly thicker than the thin yellow laminae. Thin section and SEM analyses found that the laminated crystalline crust-boundstone is mainly formed of calcite dendrites, microspars, and micrite (Fig. 6A-E, G-J). Extracellular polymeric substances (EPS), filamentous microbes (cyanobacteria?), diatoms, and some aragonite were also confirmed in fresh samples (Fig. 6I-K). Microbes and EPS mainly co-occur with micrite or even embed micritic crystals (Fig. 6I-K). Laminae with two different colors were also visible in thin sections (Fig. 6A-E), but crystal morphology and mineralogy of these two types of laminae display no prominent distinction. Most of the yellow laminae are much thin (typically less than 0.2 mm) and can cross the dendrite crystals without causing interruption (Fig. 6B, C). Some of them appear as yellow bands of about 0.5 mm thick, especially for the laminated crystalline crust-boundstone only made up of micrite (Fig. 6E).

Lime mud often covers pools with slowly flowing waters behind dams/waterfalls and similar semi-confined environments with low energy (Fig. 4B). Where present, some green microbial mats might grow on their surfaces, but does not always appear. One pronounced trend is that green microbial mats become more and more usual towards the downstream. Newly formed lime mud is much unconsolidated fine-grained carbonate sediments and prevail in Zone D, where the studied stream becomes “white”. Zone C can also produce lime mud in low-energy environments in some periods, but not as predominant elements. For example, few lime muds were also observed in F4 in June 2020 (Fig. 4G), but they disappeared in December 2020 (Fig. 4H). The lithified counterpart of the lime mud is rarely found, but where exposed, it usually manifested as curved thin beds with varying thickness (several to around twenty centimeters) and presented with coated gravels facies (Fig. 5E).

Travertine-encrusted breccia and phytoclast rudstone are also common products in both modern and fossil fluvial deposits (Figs. 4A, D, 5B, C, E). A common feature is that they are formed of clast-supported clasts fully or partly encrusted by travertines. Gravels from the former are generally sub-angular and poorly sorted, mostly varying from several centimeters to tens of centimeters. Some coated leaves and branches might occur within the travertine-encrusted breccia but not as the predominant components. Phytoclast rudstone is featured by much porous structure and contain lots of leaf and branch fragments coated by travertines. These two facies often appear together in pools with slowly flowing water and high-energy channels. One analogous facies to phytoclast rudstone is phytoherm boundstone standing out by intertwined roots encrusted by travertines (Fig. 4F), but the roots originate from trees living on the stream bank or dead tree roots in soils underlying the fluvial travertines, instead of as broken plant clasts. Further, the development of phytoherm boundstone is strictly limited, only in few waterfalls of Zone C, where fluvial travertines have been removed by erosion and collapse, and underling soils and roots are exposed.

Microbial boundstone and mixed siliciclastic-carbonate sands-gravels are not common components. Microbial boundstone is thin carbonate deposits sporadically developing on fossil travertines or human-made dams with steep to near vertical surfaces in Zones B and C (Fig. 4E). Micrite peloids are the predominant components in the microbial boundstone facies, whereas bright laminae formed of microspars are still present (Fig. 6H). Layer structures are visible in both hand samples (Fig. 4E) and thin sections (Fig. 6F), but pores and caves are well developed, much different from the compacted laminated crystalline crust-boundstone (Figs. 4A, C, 5A, 6A-E). Mixed siliciclastic-carbonate sands-gravels of about several to tens of centimeters thick can be exposed in some outcrops in Zones C and D and generally consist of sand- to granule-sized extraclasts and travertine clasts (Fig. 5E, F). Usually, beds of mixed siliciclastic-carbonate sands-gravels appear interbedded with either beds of coated gravel facies or beds of lime mud.

Sand-gravel sediments are unconsolidated siliciclastic deposits composed of sand-size to boulder-size clasts (Fig. 3A-C). They are the predominant facies covering the stream bed in Zones A and B, but can also locally occur in Zones C and D. In Zone C, the sand-gravel sediments generally partly fill some incised channels and pools (Fig. 3E, 4G-I). In contrast, even though siliciclastic granules, pebbles and cobbles have also been transported into Zone D, most of them have been fully or partly encrusted by travertines. Only not-submerged or partly eroded places expose some uncoated gravels (e.g. Fig. 7H).

4.3 Erosional micro-landforms

Although fluvial travertines widely extend in Zones C and D, most of them are not well preserved due to fluvial erosion, which not only breaks travertines and transports them downstream, but also produces some erosional micro-landforms. In the field, eight types of micro-landforms generated by fluvial erosion were discerned, including planned dams, dam breaches, incised channels, arches, pools with travertine-cemented rims, scour pools, potholes, and cut banks (Figs. 7). The former seven are the results of vertical erosion, whereas the one is controlled by lateral erosion.

Travertine dams are basic elements in Zones C and D and are generally tens of centimeters high and serval meters wide (Fig. 7A, B). However, some of them, particularly those from Zone C, are not well preserved. Although many of the dams still yield very flat top surfaces, similar to those formed in modern “terraced” travertine systems (e.g. Pentecost, 1990; Kele et al., 2011; Özkul et al., 2013), their top surfaces are characterized by recognizable planned/even erosional surfaces (Figs. 5A, 7A, B), instead of thin horizontal-layered travertines. Bare sediments composed of siliciclastic gravels and travertine clasts of varying sizes can be found in pools adjacent to these planned dams, but their top surfaces often located in a level consistent to the top surfaces of planned dams. In some cases, U-shaped notches less than 1.5 meters wide are present and are here treated as dam breaches/failures (Fig. 7B, C).

Incised channels are slightly undercutting channels developed mainly on the fluvial travertines with gentle slopes in Zone C (Fig. 7D). These channels are often shallow and display relatively high width/depth ratios (typically > 5), although local deepening existed was observed, forming some small scour pools along the channel. A few arch-like structures (here, named arches, Fig. 7E) existed in some waterfalls in Zone C. Their underlying soils and nearby travertines were removed, only preserving a steep travertine waterfall residue connected with the fluvial travertines behind. Pools near the waterfalls/cascades show also striking erosion, manifested dominantly as irregular scour pools of different sizes and sub-round potholes (Fig. 7F). Depth of these pools is usually no more than 0.5 m. Meter-scale pools with travertine-cemented rims are much special and only locally distributed in Zone D (Fig. 7G). Gravels (mainly pebbles) near the pool rims are glutted by travertines, but those in the pool center are non-cemented loose gravel sediments.

Bank erosion of the studied stream appears as cut banks (Fig. 7H), which are river-cut cliffs characterized by having concave shapes or much steep to near vertical surfaces. Those cut banks are more common in Zone D where the river beds are narrow (about several meters), compared with the wide and gently inclined river beds in Zone C (around ten meters wide).

4.4 Water chemistry and mixing model

Water data of this study were listed in Table 2 and shown in Figs. 8 and 9. White Whale and Un1 debouch warm (near 40 °C), near neutral water with high HCO_3^- (875 to 1281 mg/L), SO_4^{2-} (995 to 1265 mg/L), Ca^{2+} (549 to 658 mg/L), and Mg^{2+} (180 to 201 mg/L) contents, while the concentrations of other components in these two sites, such as F^-, Cl^-, Na^+, and K^+, are one to three orders of magnitude lower. Waters collected along the stream show a wide variability in their main physico-chemical parameters: temperature ranges from 7.9 to 29.3 °C, HCO_3^- ranges from 277 to 723 mg/L, SO_4^{2-} ranges from 47 to 1194 mg/L, Ca^{2+} range from 94 to 467 mg/L, and Mg^{2+} ranges from 16 to 170 mg/L. Pure stream water (i.e. F1, before the spring water adding) is featured by low temperature (7.9°C), slight alkaline (pH = 8.43), and relatively low HCO_3^- (277 mg/L) and Ca^{2+} (94 mg/L) concentrations, but rapid increases in HCO_3^-, SO_4^{2-}, and Ca^{2+} concentrations can be found after the input of thermal spring water, especially in F3 and F5 (Figs. 8A, 9).

All but three samples show positive calcite saturation indexes (SI_C > 1, Table 2, Fig. 8B). SI_C values of F2, F3 and Un1 are much lower, varying from 0.39 to 0.62, but their CO_2 partial pressures (log P_{CO2}) are higher than −1.8. The calculated travertine growth rates (R) are in a range from 0.06 to 6.38 cm/y. Spring water from White While exhibits the highest growth rate (6.38 cm/y, about two to three times of the precipitation rates of F5 to F8). Strikingly, spring water from Un1 only shows a precipitation rate of 0.44 cm/y, much distinct from that at White Whale. Waters from F4 to F8 present stable SI_C, log P_{CO2}, and R values without striking abrupt changes, whereas notable differences exist in water samples from F1 to F3 (Fig. 8B). The mixing model shows that continuous adding of rainwater into spring water is able to decrease SI_C, especially after the rainwater occupied ca. 70% of the mixed fluid, but the fluid mixing yields no considerable effect on log P_{CO2}, which is always in a narrow range from −1.78 to −2.16 (Fig. 10). The calculated travertine growth rate would gradually decrease during the adding to rainwater (Fig. 10).

4.5 Stable carbon and oxygen isotopes

$\delta^{13}C$ and $\delta^{18}O$ of the studied fluvial travertines are plotted in Fig. 11 and Table 3. The Bagni San Filippo fluvial travertines show much positive $\delta^{13}C$ ranging from 6.17‰ to 8.06‰ VPDB (average value: 6.75‰) and negative $\delta^{18}O$ between −10.61‰ to −8.83‰ VPDB (average value: −9.75‰). Overall, a positive correlation between $\delta^{13}C$ and $\delta^{18}O$ (R^2 = 0.6688) exists, if sample S6-1 was excluded, but the positive correlation become much weak when sample S6-1 is considered (R^2 =0.1382). Interestingly, although some modern travertines in Zone D display abnormal $\delta^{13}C$ and $\delta^{18}O$, the downstream increase in $\delta^{13}C$ (6.35‰ to 7.09‰ VPDB) and $\delta^{18}O$ (from −10.61‰ to −8.83‰) is visible (excluding sample S6-1) (Table 3).

5 Discussion

5.1 Travertine deposition controlled by hydrochemistry

In this study, travertines are quickly deposited in Zone D, but do not appear in Zones A. Such contrast is here interpreted as a result of water chemistry distinction. In general, calcite- or aragonite-saturated hot spring waters, irrespective of whether they are Ca-rich (e.g. Chafetz et al., 1991; Okumura et al., 2012; Sugihara et al., 2016) or Ca-deficiency (e.g. Renaut et al., 1999; Jones and Peng, 2014; Luo et al., 2021), are required to precipitate travertines (Pentecost, 2005). The exact saturation index for calcium carbonate precipitation is unknown, but might be at least no less than 0.48 in freshwater systems, as summarized by Pentecost (2005, his Table 25). However, even though Zone A is represented by water oversaturated with calcite (i.e. F1, SI_C = 1.07) (Table 2, Fig. 8B), no in situ calcite precipitate was formed. This might be because stream water in Zone A owns low temperatures and extremely low CO_2 partial pressure (−3.12) (Table 2), approximate to the atmospheric partial pressure of CO_2 (−3.4). In this condition, CO_2 release from the water would be very slow, no matter how turbulent the water is. Thus, its accompanied calcium carbonate precipitation might be strongly inhibited.

With the influx of spring water, stream water chemistry changed along the flow path (Fig. 8) and travertines started to be deposited in some areas (e.g. steep slopes and waterfalls), especially in Zones C and D. Waters in Zone C are affected by the visible input of hot water from Un1 and it nearby hot springs and display remarkable CO_2 degassing, as evidenced by the HCO_3^- concentration decreasing, resembling to waters in Zone D (Fig. 8B), but their corresponded Ca^{2+} variations are much distinct (Fig. 9). The calculated $\Delta Ca^{2+}/\Delta HCO_3^-$ in Zone D is near 0.5, whereas that in Zone C is only ca. 0.1. It seems that CO_2 degassing and associated travertine deposition dominate in Zone D, while Zone C exhibits strong CO_2 degassing but weak travertine deposition, in agreement with our field observation. Factors resulting in the degassing and precipitation differences between Zone C and Zone D are questionable. If we only compare F3 water and waters from Zone D (i.e. F5 to F8), we can find that the former represents water which has experienced slight CO_2 degassing (log P_{CO2} = −1.21) and shows low SI_C (0.62), while the latter have released abundant CO_2 (log P_{CO2} = −2.45 to −1.98) and are highly oversaturated with respected to calcite (SI_C = 1.43 to 1.52) (Fig. 8B). Hammer et al. (2005) found that calcite precipitation rate in a Norwegian thermal stream was near zero when SI_C was below 0.8, but it would increase dramatically if SI_C is over 0.8. Thereafter, Takashima et al. (2008) and Okumura et al. (2012) noticed similar SI_C values (about 0.8) for the initiation of recognizable travertine deposition. These suggests that the high P_{CO2} and associated low SI_C in F3 water are unlikely to guarantee high travertine precipitation rates. This is also supported by its low calculated calcite growth rate (i.e. R value) (Table 2, Fig. 8B).

However, gradual release of CO_2 in water along the flow path would increase the saturate state of calcium carbonate, because of the non-equilibrium CO_2 partial pressures between spring water and the atmosphere (e.g. Drysdale et al., 2002; Hammer et al., 2005; Arp et al., 2010; Keppel et al., 2012; Okumura et al., 2012; Arenas et al., 2014a; Sugihara et al., 2016). When the water arrives at F4, it shows nearly indistinguishable SI_C, log P_{CO2}, and R values with respect to waters from Zone D (Fig. 8B). If the travertine precipitation rate is only controlled by SI_C and log P_{CO2}, wide modern travertine deposits, like those in Zone D, should be formed in places adjacent to F4. This is, however, not in accordance with our field observations, so there might be some other factors. Basing on the diffusion boundary layer (DBL) model, calcium carbonate precipitation rate in turbulent flows is a function of temperature, Ca^{2+} concentration, P_{CO2}, DBL thickness (which is heavily governed by water velocity), and water sheet thickness (i.e. water depth) (Buhmann and Dreybrodt, 1985; Dreybrodt and Buhmann, 1991; Dreybrodt et al., 1992; Liu and Dreybrodt, 1997). The calcium carbonate precipitate rate (R_1) displays a linear relation with the difference between the actual Ca^{2+} concentration ($[Ca^{2+}]$) and the Ca^{2+} equilibrium concentration ($[Ca^{2+}]_{eq}$): $R_1 = \alpha \cdot ([Ca^{2+}] - [Ca^{2+}]_{eq})$ (Dreybrodt and Buhmann, 1991; Liu and Dreybrodt, 1997). A temperature increase from 10 to 20 °C is able to nearly double the "α" value (Liu and Dreybrodt, 1997, their Table 3). Apparently, the Ca^{2+} concentration and temperature of F4 water are lower than those of Zone D waters (Fig. 8), and these differences can at least double to triple the calcium carbonate precipitation rate in Zone D. Thus, the differential travertine deposition between Zone C and Zone D is probably affected by water temperature and Ca^{2+} concentration discrepancies.

5.2 Erosion triggered by heavy rainfall events

Notable erosional micro-landforms, unconformities, (travertine-encrusted) gravels in Zones B, C and D (Figs. 4G-I, 5) show that the studied stream also experienced episodic erosion. The studied depositional system is like a perennial stream due to the successive spring water input. Water discharges of hot springs at Bagni San Filippo might be inconstant, but as discussed previously, significant spring water adding would result in the oversaturation of calcite in water from Zones B, C and D and would clearly promote travertine deposition, instead of eroding early-formed travertines. Although some travertine waterfalls might be perched (i.e. protruded towards the flow direction) because of the travertine overgrowth on the waterfall face (Gradziński et al., 2018), like those from Azuaje, Spain (Rodríguez-Berriguete et al., 2012) and Shihuadong, China (Luo et al., 2021), and spontaneous collapse of these perched travertines can generate some travertine clasts, it is difficult to account for the occurrence of siliciclastic gravels in Zones C and D (e.g. Figs. 3C-E, 5D). These gravels are largely delivered from the upstream area by highly energetic flows, but the observed water flow conditions in Zone A in December 2020 and June 2021 (Fig. 3A, B) are not enough to carry pebbles and cobbles to Zones B, C, and D.

In fact, stream water supply from the upstream is variable at different times of the year and infiltration is present in place (e.g. Fig. 3A, B), making the stream reach before Site 2 (i.e. Zone A) similar to an ephemeral stream. The studied area owns a sub-Mediterranean climate regime, which promises seasonal changes in air temperature (warm summer and cold winter) and rainfall (mainly concentrating in Autumn and Winter) (Fig. 2A, B) and would thus affect the surface runoff condition. Although the surface runoff response to rainfall is complex and might be influenced by multiple factors, like rainfall intensity, rainfall duration, aerial extent and soil infiltration capacity (e.g. Martínez-Mena et al., 1998; Moody and Martin, 2001; Rodríguez-Blanco et al., 2012; Alexander et al., 2020), the climate controlled runoff variation is indeed present at Bagni San Filippo and nearby areas. For instance, Orcia River near Bagni San Fillippo displays relatively high water tables and frequent peaks in autumn and winter, but stable and low water tables in spring and winter (Fig. 2C). However, common rainfall events in autumn and winter do not means frequent erosion events. Short-term light rain events, for example, cannot produce enough runoff for travertine erosion probably because of the soil infiltration (Moody and Martin, 2001) and the existence of erosion/incision thresholds (i.e. boundary shear stress) (e.g. Dietrich et al., 1993; Snyder et al., 2003; DiBiase and Whipple, 2011; Scherler et al., 2017). Furthermore, considering that regular erosion was not found in Zone D, travertine erosion in Zone D might be neither seasonal nor annual, and only reflects extreme rainfalls and associated heavy flood events, like the storm/flood event in November, 2012 (generating near 300 mm precipitation within 48 hours at Abbadia San Salvatore) (Figs. 1B, 2A, C). One forceful evidence is from Fig. 7C, where the travertines formed in Stages 1 and 2 display different thicknesses and those formed in Stage 1 are too thick to be deposited within one year (i.e. annual) or several months (i.e. seasonal).

Processes contributing to fluvial bedrock erosion/incision are complicated, including dissolution, cavitation, abrasion (bedload or suspended load), and plucking/quarrying (e.g. Allen, 1971; Whipple et al., 2000; Chatanantavet and Parker, 2009; Huda and Small, 2014; Scheingross et al., 2014). All of them are expected to play some roles in the travertine erosion at Bagni San Filippo. For instance, our mixing model (Fig. 10) has shown that large amounts of rainwater adding would dilute the stream water and might lead travertine dissolution, while the presence of potholes (Fig. 7F) strongly indicate the potential influences of cavitation. The most significant processes, however, might be abrasion and plucking. Whipple et al. (2000) indicated that abrasion dominates in massive rocks with smooth surfaces, surfaces with many ripples, flutes, and potholes, or surfaces lacking exhumed joint planes, whereas plucking dominantly occurs where rock surfaces are densely jointed. In the studied system, different environments yield different surface topography and rock types. The latter can also determine the fluvial erosion rate because of the different rock tensile strengths and erosional resistances (e.g. Stock and Montgomery, 1999; Sklar and Dietrich, 2001; Zondervan et al., 2020). Overall, sufficient upstream sediment supplies during extreme storm/floods events would promise abrasion of fluvial travertines in all environments, but if the floods are not too high in discharge and/or do not carry many particles, plucking might become more common, especially in pools where the fragile lime mud can be easily quarried, and channels where the coated gravels (and phytoclasts) might be removed if there is enough shear stress.

5.3 Environments and depositional model

Present travertine deposition mainly occurs in Zone D, while Zone C also displays widespread fossil travertines flooring the stream bed (e.g. Fig. 3D, E). The basic sub-environments comprise waterfalls (e.g. Fig. 3E, G), pools (e.g. Fig. 3G), channels (e.g. Figs. 4D, 7H), and slopes (e.g. Fig. 3D). With respect to travertine waterfalls, their formation is commonly considered to be controlled by the uneven substrate and associated abnormal flow velocity and strong CO_2 degassing near the knickpoints (e.g. Guo and Riding, 1999; Florsheim et al., 2013; Özkul et al., 2014; Mors et al., 2019; Luo et al., 2021). At Bagni San Filippo, travertine waterfalls generally own a stepped structure. Such stepped structure is probably controlled by the local topography, because the original river beds probably lack steep cliffs and might contain some ramps with small irregularities, favoring the constitution of small stepped waterfalls (Arenas et al., 2014b). Formation of the pools (i.e. quiet dammed areas behind or under the waterfalls) might be provoked by the high aggradational rate (Vázquez-Urbez et al., 2012; Arenas et al., 2014b), but episodic storm/flood events might also assist their development by eroding/destroying travertines under the waterfalls (i.e. deepening the pools) and transporting them downstream.

Unlike waterfalls and pools, which were found in both Zone C and Zone D, slopes and channels are developed in Zone C and Zone D, respectively. Based on their distribution, the studied stream is here divided into two subsystems: slope-pool-waterfall subsystem (i.e. Zone C, non-active at present) and channel-pool-waterfall subsystem (i.e. Zone D, still active) (Fig. 12). Such system differentiation (i.e. slope vs channel) is largely attributed to the distinction of original stream beds. Zone C is characterized by slightly inclined and wide river beds, different from the narrow and deep channels in Zone D. In dry periods (no or little runoff/rainwater input), travertines should be precipitated in both the wide slopes and narrow channels (e.g. Fig. 13A), but conditions change if floods occur, because floods might strongly handicap travertine deposition and even erode early-formed deposits (Fig. 13B). In river systems, channel width often yields negative relationship with erosion rates (e.g. Duvall et al., 2004; Amos and Burbank, 2007; Yanites and Tucker, 2010), because of the decrease of flow velocity and water depth (assuming a stable and constant water discharge, according to the Manning Formula) (Manning et al., 1891), and accompanied lowering of the boundary shear stress and erosion capability. In this circumstance, wide beds in Zone C would experience weak erosion during flood events. On the contrary, although travertines would still be rapidly deposited in Zone D during dry periods, narrow river beds might promote fluvial erosion when there are floods. Moreover, Zone D is located in the downstream area and receives more spring water (higher discharge) than Zone C. This would, to some degree, increase the erosion potential during floods events. As a result, travertines deposited in narrow stream beds of Zone D would experience heavy erosion and are difficult for preservation, forming travertine channels covered by lots of travertine-coated gravels, travertine-coated phytoclasts, and travertine clasts (e.g. Figs. 4D, 5B, 13B), while wide, well-preserved travertine slopes might be generated in Zone C (Fig. 13B).

From the discussion above and the basic geological setting, the depositional model of fluvial travertines in the studied site can be constructed. The original stream is a conventional gravel-floored mountainous ephemeral stream with low discharges and dried river beds in most of the history due to infiltration and the dearth of surface water supply. However, a left-lateral strike-slip fault and associated small faults/fractures near Bagni San Filippo (Fig. 1B) connected the surface with the deep hydrothermal reservoirs (Brogi et al., 2010; Brogi et al., 2015), promoting thermal water upwelling and producing many hot springs characterized by Ca^{2+}- and HCO_3^--rich water. Some of these springs, especially those in the west bank of the studied stream, continuously issue thermal waters to the studied stream. The mixture of the thermal water and some (pure) stream water (with positive SI_C but much weak CO_2 degassing potentials) is still oversaturated with calcite/aragonite and shows strong CO_2 degassing potentials. As a result, fluvial travertines were deposited in the stream bed, but two different fluvial travertine-depositing subsystems, including slope-pool-waterfall subsystem and channel-pool-waterfall subsystem, were formed due to the original river bed distinction and episodic erosion. The former is largely generated by hot springs near Un1 and nearby springs, whose activity is much weak at present, but the widely distributed travertines in Zone C strongly indicate the important contribution of (paleo-)springs near Un1. The wide and slightly tilted stream beds in Zone C provided favorable conditions for the formation of travertine slopes and reinforce their resistance to subsequent fluvial erosion, while inclined slopes with small irregularities promoted the organization of small stepped waterfalls and pools. The most important spring water input point is near White While nowadays. Thus, travertine deposition is currently concentrated in places after White Whale (i.e. Zone D). Waterfalls and pools were also formed in this area due to the uneven river beds, but travertine slopes basically disappeared, because of the narrow river beds and episodic erosion. These two enhanced the capability of fluvial erosion and sediment transport during storm/flood events, resulting in the development of channels floored by travertine-coated components and finally forming a channel-pool-waterfall subsystem in Zone D.

5.4 Comparison with other fluvial travertines

Although not much information of fluvial travertines is available, they have been recorded in Aksaz (Turkey) (Özkul et al., 2014), Azuaje (Spain) (Rodríguez-Berriguete et al., 2012; Rodríguez-Berriguete and Alonso-Zarza, 2019), and Ngol (Cameroon) (Bisse et al., 2018). Here, we compared them with the studied site to discuss their depositional and erosional characteristics and formation mechanisms (Table 4). A notable common feature is that they all occur in valleys of mountainous areas, even though these valleys can be either much narrow (tens of meters in width, like the studied case, Fig. 1C) or several kilometers wide (Özkul et al., 2014). Such topographic control is definite, because surface topography rules the surface runoff distribution, and elongated low areas are required to receive spring water and form rivers/streams. In places without valleys, such as flat surfaces or terraced/smooth slopes, nearly circle-shaped or fan-shaped discharging areas would be formed, resulting in the development of mounds, fissure-ridges, slopes, or other geometries (e.g. Pentecost, 2005; Pedley, 2009; Capezzuoli et al., 2014; Della Porta, 2015). Additionally, valleys are natural water catchment areas in non-arid regions, so many fluvial travertine-depositing systems might be hot spring influenced (i.e. as the consequence of thermal spring water and river water mixing), instead of “pure hot spring rivers”. This is consistent with the field observations in Ngol (Bisse et al., 2018) and Bagni San Filippo, where hot springs emerging on nearby hills continuously pour water into the rivers. The distribution of fossil fluvial travertines and adjacent perched travertines at Azuaje also implies that this fluvial system was likely fed by perched hot springs (Rodríguez-Berriguete et al., 2012; Rodríguez-Berriguete and Alonso-Zarza, 2019). Furthermore, considering that present climate at Azuaje is drier than the period when the travertines were deposited and there is still a north-flowing river nowadays (Rodríguez-Berriguete and Alonso-Zarza, 2019), fluid mixing between the hot spring water and upstream river water during the travertine deposition can be also expected.

Hot springs depositing fluvial travertines seem to be both Ca^{2+}-rich (≥ 300 mg/L) and HCO_3^--rich (mostly ≥ 1000 mg/L) (Table 4). Although thermal waters deficient in either Ca^{2+} or HCO_3^- are able to form travertines and have been documented in many studies (e.g. Jones et al., 2000; Hochstein et al., 2010; Renaut et al., 2013; Jones and Peng, 2014; 2016; Luo et al., 2021), Ca^{2+}- and HCO_3^--rich waters provide an impetus for the development of fluvial travertines by promoting CO_2 degassing and associated travertine deposition and supporting long and large depositional areas. For instance, the flow path in Zone D is more than 300 m long, but Ca^{2+} and HCO_3^- consumption in the water is not rapid and only decrease from 467 to 350 mg/L and 723 to 497 mg/L, respectively (Table 2, Fig. 8). The water is still oversaturated with respect to calcite and would continuously precipitate calcite if there is no other fluid input. Another typical example is the Aksaz fluvial system (Turkey), which extends several kilometers long (Özkul et al., 2014). Physico-chemical characteristics of their paleo-springs are unknown, but might be similar to nearby modern hot springs features by high Ca^{2+} and HCO_3^- contents (Table 4). Moreover, to form such a "giant" fluvial travertine system, high discharges and long term hot spring activity during their formation can also be reasonably inferred.

In the above mentioned four sites, three main lithofacies types can be recognized according to their genesis and chemical compositions: carbonate facies, mixed clastic-carbonate facies, and clastic facies (Table 4). Overall, the fluvial deposits show abundant carbonate facies, containing both travertines formed in high energy environments (e.g. crystalline crust/ crystalline facies/laminated crystalline crust-boundstone) and those produced in low-energy environments (e.g. micritic travertine/laminated boundstone/lime mud) (Rodríguez-Berriguete et al., 2012; Özkul et al., 2014; Rodríguez-Berriguete and Alonso-Zarza, 2019). Only in Ngol, (pure) carbonate facies are rare and explanations were not given by Bisse et al. (2018). However, according to our findings about controls on the differences between Zone C and Zone D (Section 5.1), one reasonable explanation is that different stream reaches in Ngol received distinct spring water contributions. Clastic-carbonate facies and/or clastic facies were reported in Aksaz, Ngol, and Bagni San Filippo. Their occurrence largely reflects the episodic heavy floods/storms, as suggested by Özkul et al. (2014). Indeed, all the four fluvial systems developed in natural valleys of mountainous areas, where heavy rainfalls can induce floods easily. However, influenced by the complex conditions of fluvial systems (e.g. the distinctions of upstream sediment supply and stream power), such flood-induced erosion might also appear only as simple discontinuities within travertine sequences, like those from Azuaje (Spain) (Rodríguez-Berriguete and Alonso-Zarza, 2019), instead of the accumulation of extraclasts.

The $\delta^{13}C$ values of the fluvial travertines from the four areas mainly range from 4‰ to 8‰ (Table 4, Fig. 12), consistent with the $\delta^{13}C$ signature of representative (thermogene) travertines (Pentecost and Viles, 1994; Pentecost, 2005; Teboul et al., 2016). However, their depositional temperatures are not too high, especially for those from Bagni San Filippo (29.3 to 25.4 °C in Zone D, Table 2, Fig. 8). Using the temperature classification of spring-related carbonates of Capezzuoli et al. (2014), the Bagni San Filippo fluvial travertines seem to situate neither the "travertine" zone (generally ≥ 30 °C) nor the "tufa" zone (commonly ≤ 20°C), but no widespread macrophytes and invertebrates were found. Furthermore, the spring waters at Bagni San Filippo show visible downstream temperature decreasing (from 29.3 to 25.4 °C in Zone D) because of the low air temperatures (ca. 5 °C in winter when we measured the temperatures, Fig. 2A, B), and their Ca^{2+} (ca. 300 to 500 mg/L) and HCO_3^- (> 500 mg/L) concentrations are higher than those of typical tufa-depositing springs (Ca^{2+} < 200 mg/L, HCO_3^- < 420 mg/L) (Pentecost, 2005). Thus, the Bagni San Filippo fluvial carbonate deposits are more like travertines, instead of tufas. However, the low air temperatures, air-water P_{CO2} contrast, evaporation, and/or microbial activity, would cause the downstream water temperature decreasing and ^{13}C enrichment (e.g. Friedman, 1970; Chafetz et al., 1991; Guo et al., 1996; Kele et al., 2008; Kele et al., 2011). Consequently, "travitufas" (i.e. carbonate deposits formed in ambient temperatures and showing travertine-like ^{13}C signatures: generally > 0) (Capezzuoli et al., 2014) would be formed. In the studied case, water in Zone D flows into a lager stream (Rondinaio Creek, Fig. 1C) and travertine deposition after the confluence is variable (very weak in winter, but visible in summer, Fig. 3H, I). Our samples were all collected in February, 2021 when the carbonate deposits were deficient in places after the confluence, making it inaccessible to directly analyze the relationship between travertines and possible downstream travitufas.

However, for the well-preserved fluvial travertine systems without strong influence of climate and confluence, travitufas might occur in downstream areas. Excitingly, Rodríguez-Berriguete and Alonso-

Zarza (2019) observed some fluvial travitufa (called “tufa” in their study, showing tufa-similar petrographic features but travertine-like $\delta^{13}C$ signatures, $\delta^{13}C$ =3.60‰ to 6.11‰ VPDB) developing hundreds of meters downstream from fluvial travertines ($\delta^{13}C$ = 4.36‰ to 10.78‰) in Azuaje, Spain. Rodríguez-Berriguete et al. (2021) then reported similar fluvial travitufas in Las Temisas, and Los Verrazales (near Azuaje) and concluded two possible interpretations for their relatively low $\delta^{13}C$: i) probable disturbance processes within the aquifer or ii) after groundwater emerged at the spring. For those from Azuaje, the latter might be more reasonable, because they were formed contemporaneously with the upstream fluvial travertines (i.e. same headsprings) (Rodríguez-Berriguete and Alonso-Zarza, 2019). Based on this and the local topography (valley: natural water catchment), it is possible that water input from streams on hillsides in the lower Azuaje stretch brought some $\delta^{13}C$-depleted soil CO_2 to the river and slightly modified the $\delta^{13}C$ signature in the river water during the travitufa deposition. The paleo-temperature evaluation of the Aksaz fluvial travertines (Turkey) also found some samples with temperatures less than 20 °C (Özkul et al., 2014) and might be travitufas, but their locations and relationships with the whole system were not clear.

Although natural cold-spring “travitufas” have been described in several places (Fig. 12), such as Baishuitai (China) (Liu et al., 2003), Huanglong (China) (Wang et al., 2014), and Yerköprü (Turkey) (Delikan and Mert, 2019), the above discussions indicate that carbonates in fluvial systems should be analyzed carefully. Their $\delta^{13}C$ and $\delta^{18}O$ and possible track of their temporal and spatial distributions are required to disclose their genesis, because some “tufa-like fluvial carbonates” might be influenced by hot springs (i.e. as distal parts of hot spring influenced rivers). Additionally, when the hot spring contribution is small, spring water input might only slightly increase the water temperature, but their relatively abundant Ca^{2+} and HCO_3^- influx (compared with the original river water) would make the mixing fluid to be able to precipitate calcium carbonate. In this case, fluvial carbonates formed by hot waters (i.e. travertine) might not be existed. This phenomenon has been observed in Lúčky (Slovakia), where deeply-circulating water ascended along the faults and then mixed with stream water to form cold-water fluvial carbonate deposits (especially in waterfall environments) (Gradziński, 2010; Gradziński et al., 2015). Although the deposits were previously referred to as tufas due to their low precipitation temperatures (4.7 to 19.8 °C) (Gradziński, 2010), their $\delta^{13}C$ values (ca. −1‰ to 5‰, Fig. 11) indicate that they were influenced by hot deeply-circulating water (Gradziński et al., 2015) and might be travitufas. The Quaternary fluvial carbonate deposits from Sarıkavak (Turkey) were also interpreted as distal travitufas of a travertine system (Toker, 2017) because of their relatively positive $\delta^{13}C$ (mainly ranging from −0.5‰ to 1‰, Fig. 11) (Toker, 2017; Tagliasacchi and Kayseri-Özer, 2020), but whether they were formed by natural temperature decreasing or water input from other streams is questionable. All these indicate that some of the fluvial carbonate deposits might be connected with hot springs and possible local high thermal gradients in their upstream areas, rather than cold karst springs.

6 Conclusions

Detailed study of the modern Bagni San Filippo fluvial travertine system obtained the following conclusions:

1) The original stream at Bagni San Filippo is an ephemeral stream floored by gravel sediments and subsequent travertine deposition is mainly controlled by hot springs on the hillside, which continuously supply the stream with spring water with high Ca^{2+} and HCO_3^- concentrations.

2) Facies composition of the fluvial deposits is complex, but the most common facies only include laminated crystalline crust-boundstone, travertine-encrusted breccia, and lime mud, which mainly indicate slopes and waterfalls partly affected by micro-organisms, post-flood channels/pools, and low-energy pools, respectively.

3) The presence of notable erosional micro-landforms, unconformities, (travertine-encrusted) gravels are ascribed primarily to episodic heavy rainfall events and accompanied floods, while abrasion and plucking are considered to be dominant erosional processes.

4) Influenced by the original stream bed difference, two subsystems, including slope-pool-waterfall and channel-pool-waterfall subsystems, were formed. The former reflects travertine deposition within wide and slightly inclined stream beds and yields widespread travertines on slopes, while the latter is formed in narrow stream beds and contain many coated components in channels.

5) The comparison shows that fluvial travertines occur in valleys with existing rivers and their formation is largely related to hot springs near the valleys. The original spring waters commonly contain high Ca^{2+} and HCO_3^- concentrations and the relative contribution of spring water and river water controls

the facies composition. Water cooling along the river would move the carbonate deposition into the "travitufa" zone, indicating the significance of careful examinations of facies distribution and carbon-oxygen isotope composition in fluvial carbonate studies.

Overall, this study suggests that fluvial travertine formation is essentially the deposition of travertines in "existing" hot spring influenced rivers and is controlled by topography, hot spring contribution, and original river bed geometry, and fluvial erosion.

Acknowledgements

This work was funded by the China Scholarship Council (grant No. 201908510230 to Luo L.) and the National Natural Science Foundation of China (grant Nos. 41972116 and 41572097 to Wen H.).

Declaration of interests

The authors declare that they have no known competing financial interests or personal relationships that could have appeared to influence the work reported in this paper.

References

Alexander, J., Herbert, C.M., Fielding, C.R., Amos, K.J., 2020. Controls on channel deposits of highly variable rivers: Comparing hydrology and event deposits in the Burdekin River, Australia. Sedimentology 67, 2721-2746.

Allen, J.R.L., 1971. Transverse erosional marks of mud and rock: their physical basis and geological significance. Sedimentary Geology 5, 167-385.

Amos, C.B., Burbank, D.W., 2007. Channel width response to differential uplift. Journal of Geophysical Research: Earth Surface 112, F02010.

Arenas, C., Osácar, C., Sancho, C., Vázquez-Urbez, M., Auqué, L., Pardo, G., 2010. Seasonal record from recent fluvial tufa deposits (Monasterio de Piedra, NE Spain): sedimentological and stable isotope data. Geological Society, London, Special Publications 336, 119-142.

Arenas, C., Piñuela, L., García-Ramos, J.C., 2015. Climatic and tectonic controls on carbonate deposition in syn-rift siliciclastic fluvial systems: A case of microbialites and associated facies in the Late Jurassic. Sedimentology 62, 1149-1183.

Arenas, C., Vázquez-Urbez, M., Auqué, L., Sancho, C., Osacár, C., Pardo, G., 2014a. Intrinsic and extrinsic controls of spatial and temporal variations in modern fluvial tufa sedimentation: A thirteen-year record from a semi-arid environment. Sedimentology 61, 90-132.

Arenas, C., Vázquez-Urbez, M., Pardo, G., Sancho, C., 2014b. Sedimentology and depositional architecture of tufas deposited in stepped fluvial systems of changing slope: Lessons from the Quaternary Anamaza valley (Iberian Range, Spain). Sedimentology 61, 133-171.

Arp, G., Bissett, A., Brinkmann, N., Cousin, S., De Beer, D., Friedl, T., Mohr, K.I., Neu, T.R., Reimer, A., Shiraishi, F., Stackebrandt, E., Zippel, B., 2010. Tufa-forming biofilms of German karstwater streams: microorganisms, exopolymers, hydrochemistry and calcification. Geological Society, London, Special Publications 336, 83-118.

Bastianini, L., Rogerson, M., Mercedes-Martín, R., Prior, T.J., Cesar, E.A., Mayes, W.M., 2019. What causes carbonates to form “shrubby” morphologies? An Anthropocene limestone case study. Frontiers in Earth Science 7, 236.

Bencini, A., Duchi, V., Martini, M., 1977. Geochemistry of thermal springs of Tuscany (Italy). Chemical Geology 19, 229-252.

Bisse, S.B., Ekomane, E., Eyong, J.T., Ollivier, V., Douville, E., Maffo Nganne, M.J., Ekoko eric, B., Bitom, L.D., 2018. Sedimentological and geochemical study of the Bongongo and Ngol travertines located at the Cameroon Volcanic Line. Journal of African Earth Sciences 143, 201-214.

Brogi, A., 2004. Seismic reflection and borehole logs as tools for tectonic and stratigraphical investigations; new geological data for the Tuscan Nappe exposed in the northeastern Mt. Amiata area (Northern Apennines, Italy). Italian Journal of Geosciences 123, 189-199.

Brogi, A., Capezzuoli, E., Karabacak, V., Alcicek, M.C., Luo, L., 2021. Fissure ridges: A reappraisal of faulting and travertine deposition (travitonics). Geosciences 11, 278.

Brogi, A., Capezzuoli, E., Liotta, D., Meccheri, M., 2015. The Tuscan Nappe structures in the Monte Amiata geothermal area (central Italy): a review. Italian Journal of Geosciences 134, 219-236.

Brogi, A., Fabbrini, L., 2009. Extensional and strike-slip tectonics across the Monte Amiata–Monte Cetona transect (Northern Apennines, Italy) and seismotectonic implications. Tectonophysics 476, 195-209.

Brogi, A., Liotta, D., Meccheri, M., Fabbrini, L., 2010. Transtensional shear zones controlling volcanic eruptions: the Middle Pleistocene Mt Amiata volcano (inner Northern Apennines, Italy). Terra Nova 22, 137-146.

Buhmann, D., Dreybrodt, W., 1985. The kinetics of calcite dissolution and precipitation in geologically relevant situations of karst areas: 1. Open system. Chemical Geology 48, 189-211.

Capezzuoli, E., Brogi, A., Ricci, M., Bertini, A., 2011. Travertines and calcareous tufa in southern Tuscany (central Italy). Field Trip Guide book of ISTT (International school of travertine and tufa). Ed. Il Campano, Pisa 66.

Capezzuoli, E., Gandin, A., Pedley, M., 2014. Decoding tufa and travertine (fresh water carbonates) in the sedimentary record: The state of the art. Sedimentology 61, 1-21.

Chafetz, H., Rush, P.F., Utech, N.M., 1991. Microenvironmental controls on mineralogy and habit of $CaCO_3$ precipitates: an example from an active travertine system. Sedimentology 38, 107-126.

Chatanantavet, P., Parker, G., 2009. Physically based modeling of bedrock incision by abrasion, plucking, and macroabrasion. Journal of Geophysical Research: Earth Surface 114, F04018.

Chiodini, G., Cardellini, C., Caliro, S., Avino, R., Donnini, M., Granieri, D., Morgantini, N., Sorrenti, D., Frondini, F., 2020. The hydrothermal system of Bagni San Filippo (Italy): fluids circulation and CO_2 degassing. Italian Journal of Geosciences 139, 1-15.

Conti, P., Cornamusini, G., Carmignani, L., 2020. An outline of the geology of the Northern Apennines (Italy), with geological map at 1: 250,000 scale. Italian Journal of Geosciences 139, 149-194.

Delikan, A., Mert, M., 2019. Depositional and geochemical characteristics of geomorphologically controlled recent tufa deposits on the Göksü River in Yerköprü (Konya, southern Turkey). Carbonates and Evaporites 34, 441-459.

Della Porta, G., 2015. Carbonate build-ups in lacustrine, hydrothermal and fluvial settings: comparing depositional geometry, fabric types and geochemical signature. Geological Society, London, Special Publications 418, 17-68.

Della Porta, G., Hoppert, M., Hallmann, C., Schneider, D., Reitner, J., 2021. The influence of microbial mats on travertine precipitation in active hydrothermal systems (Central Italy). The Depositional Record 00, 1-45.

DiBiase, R.A., Whipple, K.X., 2011. The influence of erosion thresholds and runoff variability on the relationships among topography, climate, and erosion rate. Journal of Geophysical Research: Earth Surface 116, F04036.

Dietrich, W.E., Wilson, C.J., Montgomery, D.R., McKean, J., 1993. Analysis of Erosion Thresholds, Channel Networks, and Landscape Morphology Using a Digital Terrain Model. The Journal of Geology 101, 259-278.

Dreybrodt, W., Buhmann, D., 1991. A mass transfer model for dissolution and precipitation of calcite from solutions in turbulent motion. Chemical Geology 90, 107-122.

Dreybrodt, W., Buhmann, D., Michaelis, J., Usdowski, E., 1992. Geochemically controlled calcite precipitation by CO_2 outgassing: Field measurements of precipitation rates in comparison to theoretical predictions. Chemical Geology 97, 285-294.

Drysdale, R., Gillieson, D., 1997. Micro-erosion meter measurements of travertine deposition rates: A case study from Louie Creek, northwest Queensland, Australia. Earth Surface Processes and Landforms 22, 1037-1051.

Drysdale, R.N., Taylor, M.P., Ihlenfeld, C., 2002. Factors controlling the chemical evolution of travertine-depositing rivers of the Barkly karst, northern Australia. Hydrological Processes 16, 2941-2962.

Duchi, V., Minissale, A., Paolieri, M., Prati, F., Valori, A., 1992. Chemical relationship between discharging fluids in the Siena-Radicofani graben and the deep fluids produced by the geothermal fields of Mt Amiata, Torre Alfina and Latera (Central Italy). Geothermics 21, 401-413.

Duchi, V., Minissale, A.A., Prati, F., 1987. Chemical composition of thermal springs, cold springs, streams, and gas vents in the Mt. Amiata geothermal region (Tuscany, Italy). Journal of Volcanology and Geothermal Research 31, 321-332.

Duvall, A., Kirby, E., Burbank, D., 2004. Tectonic and lithologic controls on bedrock channel profiles and processes in coastal California. Journal of Geophysical Research: Earth Surface 109, F03002.

Florsheim, J.L., Ustin, S.L., Tang, Y., Di, B., Huang, C., Qiao, X., Peng, H., Zhang, M., Cai, Y., 2013. Basin-scale and travertine dam-scale controls on fluvial travertine, Jiuzhaigou, southwestern China. Geomorphology 180, 267-280.

Ford, T.D., Pedley, H.M., 1996. A review of tufa and travertine deposits of the world. Earth-Science Reviews 41, 117-175.

Friedman, I., 1970. Some investigations of the deposition of travertine from Hot Springs—I. The isotopic chemistry of a travertine-depositing spring. Geochimica et Cosmochimica Acta 34, 1303-1315.

Frondini, F., Caliro, S., Cardellini, C., Chiodini, G., Morgantini, N., Parello, F., 2008. Carbon dioxide degassing from Tuscany and Northern Latium (Italy). Global and Planetary Change 61, 89-102.

Gradziński, M., 2010. Factors controlling growth of modern tufa: Results of a field experiment. Geological Society, London, Special Publications 336, 143-191.

Gradziński, M., Bella, P., Holúbek, P., 2018. Constructional caves in freshwater limestone: A review of their origin, classification, significance and global occurrence. Earth-Science Reviews 185, 179-201.

Gradziński, M., Wróblewski, W., Bella, P., 2015. Cenozoic freshwater carbonates of the Central Carpathians (Slovakia): facies, environments, hydrological control and depositional history. Guidebook for

Field Trips Accompanying 31st IAS Meeting of Sedimentology Held in Kraków on 22nd–25th of June 2015, 217-245.

Guo, L., Andrews, J., Riding, R., Dennis, P., Dresser, Q., 1996. Possible microbial effects on stable carbon isotopes in hot-spring travertines. Journal of Sedimentary Research 66, 468-473.

Guo, L., Riding, R., 1999. Rapid facies changes in Holocene fissure ridge hot spring travertines, Rapolano Terme, Italy. Sedimentology 46, 1145-1158.

Hammer, Ø., Jamtveit, B., Benning, L.G., Dysthe, D.K., 2005. Evolution of fluid chemistry during travertine formation in the Troll thermal springs, Svalbard, Norway. Geofluids 5, 140-150.

Hochstein, M., Simanjuntak, J., Sudarman, S., 2010. Geothermal prospects of the eastern Banda Arc Islands (Indonesia), Proceedings World Geothermal Congress, Bali, Indonesia.

Huda, S.A., Small, E.E., 2014. Modeling the effects of bed topography on fluvial bedrock erosion by saltating bed load. Journal of Geophysical Research: Earth Surface 119, 1222-1239.

Jones, B., Peng, X., 2014. Signatures of biologically influenced $CaCO_3$ and Mg-Fe silicate precipitation in hot springs: Case study from the Ruidian geothermal area, western Yunnan Province, China. Sedimentology 61, 56-89.

Jones, B., Peng, X., 2016. Mineralogical, crystallographic, and isotopic constraints on the precipitation of aragonite and calcite at Shiqiang and other hot springs in Yunnan Province, China. Sedimentary Geology 345, 103-125.

Jones, B., Renaut, R.W., 2010. Chapter 4 Calcareous spring deposits in continental settings. In: A.M. Alonso-Zarza, L.H. Tanner (Eds.), Developments in Sedimentology. Elsevier, Amsterdam, pp. 177-224.

Jones, B., Renaut, R.W., Rosen, M.R., 2000. Trigonal dendritic calcite crystals forming from hot spring waters at Waikite, North Island, New Zealand. Journal of Sedimentary Research 70, 586-603.

Kandemir, R., Tagliasacchi, E., Kayseri Özer, M., ŞAfak, D., Köroğlu, F., Hu, H.-M., Shen, C.-C., 2021. The multidisciplinary approaches on facies developments and depositional systems of the Bahçecik travertines, Gümüşhane, NE-Turkey. Turkish Journal of Earth Sciences 30, 561-579.

Kele, S., Breitenbach, S.F.M., Capezzuoli, E., Meckler, A.N., Ziegler, M., Millan, I.M., Kluge, T., Deák, J., Hanselmann, K., John, C.M., Yan, H., Liu, Z., Bernasconi, S.M., 2015. Temperature dependence of oxygen- and clumped isotope fractionation in carbonates: A study of travertines and tufas in the 6–95°C temperature range. Geochimica et Cosmochimica Acta 168, 172-192.

Kele, S., Demény, A., Siklosy, Z., Németh, T., Tóth, M., Kovács, M.B., 2008. Chemical and stable isotope composition of recent hot-water travertines and associated thermal waters, from Egerszalók, Hungary: Depositional facies and non-equilibrium fractionation. Sedimentary Geology 211, 53-72.

Kele, S., Özkul, M., Fórizs, I., Gökgöz, A., Baykara, M.O., Alçiçek, M.C., Németh, T., 2011. Stable isotope geochemical study of Pamukkale travertines: New evidences of low-temperature non-equilibrium calcite-water fractionation. Sedimentary Geology 238, 191-212.

Keppel, M.N., Post, V.E.A., Love, A.J., Clarke, J.D.A., Werner, A.D., 2012. Influences on the carbonate hydrochemistry of mound spring environments, Lake Eyre South region, South Australia. Chemical Geology 296-297, 50-65.

Kluge, T., John, C.M., Boch, R., Kele, S., 2018. Assessment of factors controlling clumped isotopes and $\delta^{18}O$ values of hydrothermal vent calcites. Geochemistry, Geophysics, Geosystems 19, 1844-1858.

Liu, Z., Dreybrodt, W., 1997. Dissolution kinetics of calcium carbonate minerals in H_2O-CO_2 solutions in turbulent flow: The role of the diffusion boundary layer and the slow reaction $H_2O + CO_2 \rightarrow H^+ + HCO_3^-$. Geochimica et Cosmochimica Acta 61, 2879-2889.

Liu, Z., Zhang, M., Li, Q., You, S., 2003. Hydrochemical and isotope characteristics of spring water and travertine in the Baishuitai area (SW China) and their meaning for paleoenvironmental reconstruction. Environmental Geology 44, 698-704.

Luo, L., Wen, H., Capezzuoli, E., 2021. Travertine deposition and diagenesis in Ca-deficiency perched hot spring systems: A case from Shihuadong, Tengchong, China. Sedimentary Geology 414, 105827.

Mancini, A., Capezzuoli, E., Erthal, M., Swennen, R., 2019. Hierarchical approach to define travertine depositional systems: 3D conceptual morphological model and possible applications. Marine and Petroleum Geology 103, 549-563.

Manning, R., Griffith, J.P., Pigot, T., Vernon-Harcourt, L.F., 1891. On the flow of water in open channels and pipes. Transactions of the Institution of Civil Engineers of Ireland 20, 161-207.

Marroni, M., Moratti, G., Costantini, A., Conticelli, S., Benvenuti, M.G., Pandolfi, L., Bonini, M., Cornamusini, G., Laurenzi, M.A., 2015. Geology of the Monte Amiata region, Southern Tuscany, Central Italy. Italian Journal of Geosciences 134, 171-199.

Martínez-Mena, M., Albaladejo, J., Castillo, V.M., 1998. Factors influencing surface runoff generation in a Mediterranean semi-arid environment: Chicamo watershed, SE Spain. Hydrological Processes 12, 741-754.

Minissale, A., 2004. Origin, transport and discharge of CO_2 in central Italy. Earth-Science Reviews 66, 89-141.

Moody, J.A., Martin, D.A., 2001. Post-fire, rainfall intensity–peak discharge relations for three mountainous watersheds in the western USA. Hydrological Processes 15, 2981-2993.

Mors, R.A., Astini, R.A., Gomez, F.J., 2019. Coexisting active travertines and tufas in the southeastern border of the Puna plateau. Sedimentary Geology 389, 200-217.

Mosello, R., Brizzio, M.C., Kotzias, D., Marchetto, A., Rembges, D., Tartari, G., 2002. The chemistry of atmospheric deposition in Italy in the framework of the National Programme for Forest Ecosystems Control (CONECOFOR). Journal of Limnology 61, 77-92.

Okumura, T., Takashima, C., Shiraishi, F., Akmaluddin, Kano, A., 2012. Textural transition in an aragonite travertine formed under various flow conditions at Pancuran Pitu, Central Java, Indonesia. Sedimentary Geology 265, 195-209.

Özkul, M., Gökgöz, A., Kele, S., Baykara, M.O., Shen, C.-C., Chang, Y.-W., Kaya, A., Hançer, M., Aratman, C., Akın, T., Örü, Z., 2014. Sedimentological and geochemical characteristics of a fluvial travertine: A case from the eastern Mediterranean region. Sedimentology 61, 291-318.

Özkul, M., Kele, S., Gökgöz, A., Shen, C.-C., Jones, B., Baykara, M.O., Fórizs, I., Németh, T., Chang, Y.-W., Alçiçek, M.C., 2013. Comparison of the Quaternary travertine sites in the Denizli extensional basin based on their depositional and geochemical data. Sedimentary Geology 294, 179-204.

Parkhurst, D.L., Appelo, C.A.J., 2013. Description of input and examples for PHREEQC version 3: a computer program for speciation, batch-reaction, one-dimensional transport, and inverse geochemical calculations: U.S. Geological Survey Techniques and Methods, book 6, chap. A43, 497 p. 6-A43.

Pattelli, G., Rimondi, V., Benvenuti, M., Chiarantini, L., Colica, A., Costagliola, P., Benedetto, F.D., Lattanzi, P., Paolieri, M., Rinaldi, M., 2014. Effects of the November 2012 Flood Event on the mobilization of Hg from the Mount Amiata Mining District to the sediments of the Paglia River Basin. Minerals 4, 241-256.

Pedley, H.M., 1990. Classification and environmental models of cool freshwater tufas. Sedimentary Geology 68, 143-154.

Pedley, M., 2009. Tufas and travertines of the Mediterranean region: a testing ground for freshwater carbonate concepts and developments. Sedimentology 56, 221-246.

Pentecost, A., 1990. The formation of travertine shrubs: Mammoth hot springs, Wyoming. Geological Magazine 127, 159–168.

Pentecost, A., 2005. Travertine. Springer, Berlin.

Pentecost, A., Viles, H., 1994. A review and reassessment of travertine classification. Géographie physique et Quaternaire 48, 305–314.

Renaut, R.W., Jones, B., Turdu, C.L., 1999. Calcite lilypads and ledges at Lorusio Hot Springs, Kenya Rift Valley. Canadian Journal of Earth Sciences 36, 649-666.

Renaut, R.W., Owen, R.B., Jones, B., Tiercelin, J.-J., Tarits, C., Ego, J.K., Konhauser, K.O., 2013. Impact of lake-level changes on the formation of thermogene travertine in continental rifts: Evidence from Lake Bogoria, Kenya Rift Valley. Sedimentology 60, 428-468.

Rodríguez-Berriguete, Á., Alonso-Zarza, A.M., 2019. Controlling factors and implications for travertine and tufa deposition in a volcanic setting. Sedimentary Geology 381, 13-28.

Rodríguez-Berriguete, Á., Alonso-Zarza, A.M., Cabrera, M.C., Rodriguez-Gonzalez, A., 2012. The Azuaje travertine: an example of aragonite deposition in a recent volcanic setting, N Gran Canaria Island, Spain. Sedimentary Geology 277, 61-71.

Rodríguez-Berriguete, Á., Camuera, J., Alonso-Zarza, A.M., 2021. Carbonate tufas as archives of climate and sedimentary dynamic in volcanic settings, examples from Gran Canaria (Spain). Sedimentology, doi: 10.1111/sed.12908.

Rodríguez-Blanco, M., Taboada-Castro, M., Taboada-Castro, M., 2012. Rainfall–runoff response and event-based runoff coefficients in a humid area (northwest Spain). Hydrological Sciences Journal 57, 445-459.

Scheingross, J.S., Brun, F., Lo, D.Y., Omerdin, K., Lamb, M.P., 2014. Experimental evidence for fluvial bedrock incision by suspended and bedload sediment. Geology 42, 523-526.

Scherler, D., DiBiase, R.A., Fisher, G.B., Avouac, J.-P., 2017. Testing monsoonal controls on bedrock river incision in the Himalaya and Eastern Tibet with a stochastic-threshold stream power model. Journal of Geophysical Research: Earth Surface 122, 1389-1429.

Sklar, L.S., Dietrich, W.E., 2001. Sediment and rock strength controls on river incision into bedrock. Geology 29, 1087-1090.

Snyder, N.P., Whipple, K.X., Tucker, G.E., Merritts, D.J., 2003. Importance of a stochastic distribution of floods and erosion thresholds in the bedrock river incision problem. Journal of Geophysical Research: Solid Earth 108, 2117.

Stock, J.D., Montgomery, D.R., 1999. Geologic constraints on bedrock river incision using the stream power law. Journal of Geophysical Research: Solid Earth 104, 4983-4993.

Sugihara, C., Yanagawa, K., Okumura, T., Takashima, C., Harijoko, A., Kano, A., 2016. Transition of microbiological and sedimentological features associated with the geochemical gradient in a travertine mound in northern Sumatra, Indonesia. Sedimentary Geology 343, 85-98.

Tagliasacchi, E., Kayseri-Özer, M.S., 2020. Multidisciplinary approach for palaeoclimatic signals of the non-marine carbonates: The case of the Sarıkavak tufa deposits (Afyon, SW-Turkey). Quaternary International 544, 41-56.

Takashima, C., Kano, A., Naganuma, T., Tazaki, K., 2008. Laminated iron texture by iron-oxidizing bacteria in a calcite travertine. Geomicrobiology Journal 25, 193-202.

Tassi, F., Fiebig, J., Vaselli, O., Nocentini, M., 2012. Origins of methane discharging from volcanic-hydrothermal, geothermal and cold emissions in Italy. Chemical Geology 310-311, 36-48.

Tchouatcha, M.S., Kouske, A.P., Takojio Nguemo, R.E., Ganno, S., Kouonang Tchounang, S., Kono, L.D., Ngonlep Miyemeck, V.T., Asah, M.F., Njinchuki, D.N., 2018. The active thermogene travertine deposits along the Cameroon volcanic line (CVL), central africa: Petrology and insights for neotectonics and paleoenvironmental approach. Journal of African Earth Sciences 144, 1-16.

Teboul, P.-A., Durlet, C., Gaucher, E.C., Virgone, A., Girard, J.-P., Curie, J., Lopez, B., Camoin, G.F., 2016. Origins of elements building travertine and tufa: New perspectives provided by isotopic and geochemical tracers. Sedimentary Geology 334, 97-114.

Toker, E., 2017. Quaternary fluvial tufas of Sarıkavak area, southwestern Turkey: Facies and depositional systems. Quaternary International 437, 37-50.

Toker, E., Kayseri-Özer, M.S., Özkul, M., Kele, S., 2015. Depositional system and palaeoclimatic interpretations of Middle to Late Pleistocene travertines: Kocabaş, Denizli, south-west Turkey. Sedimentology 62, 1360-1383.

Vázquez-Urbez, M., Arenas, C., Pardo, G., 2012. A sedimentary facies model for stepped, fluvial tufa systems in the Iberian Range (Spain): the Quaternary Piedra and Mesa valleys. Sedimentology 59, 502-526.

Wang, H., Yan, H., Liu, Z., 2014. Contrasts in variations of the carbon and oxygen isotopic composition of travertines formed in pools and a ramp stream at Huanglong Ravine, China: Implications for paleoclimatic interpretations. Geochimica et Cosmochimica Acta 125, 34-48.

Whipple, K.X., Hancock, G.S., Anderson, R.S., 2000. River incision into bedrock: Mechanics and relative efficacy of plucking, abrasion, and cavitation. GSA Bulletin 112, 490-503.

Wolthers, M., Nehrke, G., Gustafsson, J.P., Van Cappellen, P., 2012. Calcite growth kinetics: Modeling the effect of solution stoichiometry. Geochimica et Cosmochimica Acta 77, 121-134.

Yanites, B.J., Tucker, G.E., 2010. Controls and limits on bedrock channel geometry. Journal of Geophysical Research: Earth Surface 115, F04019.

Zondervan, J.R., Stokes, M., Boulton, S.J., Telfer, M.W., Mather, A.E., 2020. Rock strength and structural controls on fluvial erodibility: Implications for drainage divide mobility in a collisional mountain belt. Earth and Planetary Science Letters 538, 116221.

Figure captions

Fig. 1. (A) Simplified geological map of Tuscany and surrounding areas, showing the distribution of strata and the location of the studied area, modified from Conti et al. (2020). (B) Geological map of Bagni San Filippo and surrounding areas, modified from Brogi et al. (2015) and public data from Regione Toscana (www.regione.toscana.it/-/risorse). (C) Google map of the studied area, showing the sampling sites, the zone division, and the locations of main springs (pink squares) and (unstable) small springs (pink circles) along the stream. ASS = Abbadia San Salvatore rain gauging station, MAS = Monte Amiata Scalo stream gauging station, MR = Rufeno Mt.

Fig. 2 (A) Variations of average air temperature and meteoric precipitation in Amiata Mt. from 2010 to 2020. (B) Close up of the variation in air temperature and meteoric precipitation in Amiata Mt. in 2020. (C) Water level change of Orcia River from 2010 to 2020. Air temperature and precipitation data from the Abbadia San Salvatore rain gauging station and water table data from the Monte Amiata Scalo stream gauging station (Settore Idrologico e Geologico Regionale – Regione Toscana; www.sir.toscana.it). Air temperature and precipitation data from Feb. 2015 to March 2015 and from July 2015 to Jan. 2016 were not recorded. The station locations can be found in Fig. 1A.

Fig. 3 (A) Gravel sediments and stream water infiltration in Zone A (taken on 2020/12/22). (B) Fluvial gravels and the dry stream bed (taken on 2021/06/24). (C) Water seeping and reappearance of stream water at F2. (D) Fossil fluvial travertines with a gentle slope. (E) Fossil fluvial travertines made up of several terraces. (F) Southeast corner of White Whale and the input of thermal water. (G) Northeast corner of White Whale, showing the abundant input of thermal water. (H) Confluence of the studied stream (left) and a larger stream (left), showing the weaken of travertine deposition after the confluence (taken on 2021/02/04). (I) Confluence of the studied stream (left) and a larger stream (left), showing the visible travertine deposition after the meeting of the two streams (taken on 2021/06/24). Detailed locations can be found in Fig. 1C.

Fig. 4 Modern fluvial deposits from the area with strong hot spring contribution (A-D) and that with weak hot spring contribution (E-H). (A) Modern travertine waterfall formed of compacted laminated crystalline crust-boundstone. (B) Pool filled by lime mud with microbial mat growing on the deposit surface. (C) Travertine-encrusted gravels (red arrow) in an active pool and nearby waterfall consisting of laminated crystalline crust-boundstone. (D) Branches, leaves, and gravels (partly) coated by travertines in a narrow channel. (E) Newly formed microbial boundstone formed on a waterfall. (F) Roots encrusted by travertines below a waterfall. (G) Sand-gravel sediments and some lime muds (taken on 2020/06/19). (H) Disappearance of lime muds at the sample place of Fig. 7G (taken on 2020/12/12). (I) Gravels filling in incised channels (red arrow) and pools (white arrow).

Fig. 5 Recently formed and fossil fluvial deposits. (A) Eroded travertine waterfall composed of slightly curved laminated crystalline crust-boundstone. (B) Phytoclast rudstone and an incised channel filled by travertine-encrusted breccia and laminated crystalline crust boundstone. (C) Travertine-encrusted breccia and phytoclast rudstone. (D) Siliciclastic gravels partially coated by travertines (red arrow), travertine clasts (white arrow), and some newly formed travertines accumulated in the inclined river channel. (E) Alteration of travertine-encrusted breccia and (lithified) lime mud in the lower and middle parts and mixed siliciclastic-carbonate sands-gravels mixed siliciclastic-carbonate sands-gravels composed of siliciclastic sands and gravels and some travertine clasts (upper part). (F) Enlarged view of the mixed siliciclastic-carbonate sands-gravels. Abbreviation: Pr = phytoclast rudstone, TB = travertine-encrusted breccia, LCB = laminated crystalline crust-boundstone, MSS = mixed siliciclastic-carbonate sands-gravels.

Fig. 6 Thin section photos (A-F) and backscattered-electron microphotographs (G-K) of laminated crystalline crust-boundstone (A-E, G-K) and microbial boundstone (F) from the newly formed fluvial travertines (A-B, E-K) and fossil travertines (C-D). (A) Dendritic crystals growing on a yellow growth lamina (red arrow). (B) Yellow growth laminae (red arrows) across dendritic crystals but causing no crystal interruption. (C) Closely spaced yellow growth laminae (red arrows) across dendritic crystals. (D, E) Laminated crystalline crust-boundstone made up of microspars of about several tens of micrometers (F) or micrite mostly less than 10 μm in diameter (G), but show recognizable thin (F) and thick (G) yellow growth laminae. (F) Microbial boundstone composed of micrite peloids and some bright microspar laminae (red arrow). (G) Calcite dendrite and micrite crystals. (H) Calcite dendrite growing on aragonite needle aggregates (bottom left corner). (I) Calcite micritic crystals embedded in EPS and some diatoms and filamentous microbes (red arrows). (J) Aragonite and some filamentous microbes scattered among calcite micritic crystals. (K) Enlarged view of dumbbell-like and spherulitic aggregates of aragonite crystals.

Fig. 7 Erosional features and products in the studied fluvial system. (A) Planed dam (red arrow) and its behind pool filled by siliciclastic gravels and travertine clasts. (B) Dam breaches and active travertine deposition within the breaches and adjacent pools. (C) Multi-stage travertine deposition and erosion of a dam. (D) Incised channel with some siliciclastic gravels. (E) Arch formed by differential downcutting of fluvial travertines and their underlying soils. Note the residual waterfall travertine. (F) Pothole, scour pools with a few gravels (white arrow), and planed dam with an even erosion top surface (red arrow). (G) Pool with travertine-cemented rims characterized by travertine-cemented gravels in the pool rim and the gravels without cementation in the pool center. (H) Cliff bank which is experiencing lateral erosion and collapse. Black arrows indicate the flow direction.

Fig. 8 (A) Evolution of temperature, and Ca^{2+} and HCO_3^- concentrations along the stream. (B) Variations of calcite saturation indexes (SI_C), CO_2 partial pressures (log P_{CO2}), and simulated calcite precipitation rates (R) using the process-based calcite growth model from Wolthers et al. (2012, their Eq. 34) along the studied stream.

Fig. 9 Correlation between Ca^{2+} concentration and HCO_3^- concentration of waters from the studied stream and adjacent hot springs.

Fig. 10 Variations of saturation index of calcite (SI_C), partial pressure of CO_2 (log P_{CO2}), and calculated travertine growth rate (R) during the mixing of spring water from White While and rainwater (T = 20°C) from Monte Rufeno (ca. 20 km away from the studied area, Fig. 1A) (Mosello et al., 2002). The original water data can be found in Table 1. The saturation index line of calcite precipitation in freshwater systems is from Pentecost (2005, his Table 25).

Fig. 11 Plot of the stable carbon and oxygen isotope values of the studied fluvial travertine at Bagni San Filippo, in comparison with fluvial travertines from Azuaje (Spain) (Rodríguez-Berriguete et al., 2012), Aksaz (Turkey) (Özkul et al., 2014), and Ngol (Cameroon) (Bisse et al., 2018), fluvial travitufas from Azuaje (Spain) (Rodríguez-Berriguete and Alonso-Zarza, 2019), Sarıkavak (Turkey) (Toker, 2017; Tagliasacchi and Kayseri-Özer, 2020), and Lúčky (Slovakia) (Gradziński et al., 2015), and non-fluvial travitufas from Baishuitai (China) (Liu et al., 2003), Huanglong (China) (Wang et al., 2014), and Yerköprü (Delikan and Mert, 2019). Note that some data from Ngol (Cameroon) might be from non-fluvial travertine deposits because of the lacking of sampling sites. $\delta^{13}C$ ranges of typical thermogene travertines (i.e. travertine) and meteogene travertines (i.e. tufa) are from Pentecost and Viles (1994)

Fig. 12 Schematic block diagram of the studied fluvial system, showing the influence of original river bed features on the development of slopes and channels.

Fig. 13 (A) Schematic deposition model of the studied hot spring controlled stream in dry period, showing the continuous travertine deposition of crystalline crust-boundstone in high-energy waterfalls and lime muds in pools. (B) Erosional model of the studied stream during extreme flood events, showing the erosion of early formed travertines (especially those in slopes, channels, and top parts of waterfalls) and deposition of gravels.

Table captions

Table 1 Characteristics and environmental interpretations of the main facies recognized in the studied fluvial deposits. Abbreviation: A = abundant, C = common, R = rare.

Table 2 Water chemistry of the studied hot springs and stream at Bagni San Filippo and rain water from Monte Rufeno. * without official name; # data from Mosello et al. (2002).

Table 3 Stable C-O isotopic composition of the studied fluvial travertines at Bagni San Filippo, Italy.

Table 4 General characteristics of the studied fluvial travertines and possible headsprings (Chiodini et al., 2020), in comparison with those from Aksaz (Turkey) (Özkul et al., 2014), Azuaje (Spain) (Rodríguez-Berriguete et al., 2012; Rodríguez-Berriguete and Alonso-Zarza, 2019), and Ngol (Cameroon) (Bisse et al., 2018; Tchouatcha et al., 2018). Question marks (?) indicate the information not indicated clearly by the previous researchers or deduced from their description.

Table 1 Characteristics and environmental interpretations of the main facies recognized in the studied fluvial deposits. Abbreviation: A = abundant, C = common, R = rare.

Facies	Description	Interpretation and environment	Zone and abundance
Laminated crystalline crust-boundstone (Figs. 7A, C, 8A)	Compacted flat to wavy laminated travertine deposits. Notable bright laminae mainly ranging from ca. 1 to 10 mm thick and alternating yellow laminae generally less than 1 mm in modern deposits, but lacking apparent color distinction in fossil deposits. Mainly composed of dendritic crystals, microspars, and micrite	Turbulence-induced rapid CO_2 degassing and fast travertine deposition on waterfalls and slopes. Microbes and their secreting EPS might server as nucleation points and aid for the formation of micrite and microspars in local environments with relatively slowly flowing water, but very fast flowing water inhibited microbial colonization, producing dendritic crystals	
Lime mud (Fig. 7B, 8E)	Soft white fine carbonate sediments. Green mats can partially cover the lime mud, especially in the downstream area	Slow deposition in low-energy pools with water supersaturated with calcite, but might be promoted microbial activities	
Microbial boundstone facies (Fig. 7E)	Porous carbonate crusts with undulated patterns. Dominantly made up of micritic peloids but also containing some and local	Micritic peloids suggest their genetic relation with microbes, while bright microspars might indicate local strengthen of abiotic precipitation. Appearing in slopes and waterfalls with fast flowing water	

	discontinuous laminae formed of microspars	
Phytoherm boundstone (Fig. 7F)	Carbonate deposits developing on roots and continued encrusting the roots	Water dripped from waterfalls hits the roots and forms splashing areas, accelerating CO_2 release and travertine precipitation around the roots. Occurring in few waterfalls and their splash areas
Travertine-encrusted breccia (Figs. 7B, 8B, C, E)	Clast-supported siliciclastic gravels in varying size and encrusted by travertine. Probably containing some siliciclastic sands and travertine clasts	Eroded siliciclastic gravels transported by high-energy flows during floods and redeposited in pools and channels. Hot water supersaturated with calcite then directly precipitated travertines around them and formed outer encrusts
Phytoclast rudstone (Fig. 7D, 8B, C)	Porous clast-supported phytoclasts encrusted by travertine. Phytoclasts are mainly composed of leaf and twig fragments	Leaves and branches from surrounding environments or plant fragments transported from upper stream accumulated in pools and dammed areas in channels and subsequently experienced travertine encrustation
Mixed siliciclastic-carbonate sand-gravels (Fig. 8E, F)	Loose, structureless mixed deposits composed of siliciclastic sand-gravels and travertine clasts. Most of the particles are several millimeters (sand- to granule-sized) in diameter	Relatively high discharge and turbulent water during floods broke recently formed travertines (especially lime mud) and transported them and some millimeter-scale gravels and sands to pools
Sand-gravel sediment (Fig. 7G, H)	Coarse clast-supported detrital sediments mainly	Eroded gravels transported by high-energy flows during floods and re-deposited in channels and pools

		made up of siliciclastic gravels and sands. Might contain some travertine clasts (especially in the downstream area of Zone D)	in Zones A to C, where travertines cannot be or can only slowly precipitated.

Table 2 Water chemistry of the studied hot springs and stream at Bagni San Filippo and rain water from Monte Rufeno. * without official name; # data from Mosello et al. (2002).

Location	T (°C)	pH	TDS (ppm)	HCO_3^- (mg/L)	SO_4^{2-} (mg/L)	F^- (mg/L)	Cl^- (mg/L)	NO_3^- (mg/L)	Ca^{2+} (mg/L)	Mg^{2+} (mg/L)	Na^+ (mg/L)	K^+ (mg/L)	NH_4^+ (mg/L)	SI_C	log P_{CO2}	R (cm/y)
Thermal spring system																
Un1*	0.5	.27	1565	1281	995	2.8	16	0.2	658	180	34	12.9	1.7	0.55	−0.15	0.44
White Whale	8.9	.70	1754	875	1265	0.6	[illegible]	0.2	549	201	30	9.5	1.5	1.69	−1.78	6.38
Fluvial system																
F1	.9	.43	329	277	[illegible]	0.1	41	0.3	94	16	28	2.4	0.1	1.07	−3.12	0.60
F2	1.2	.32	582	[illegible]	120	0.4	27	0.4	157	32	23	2.4	0.1	0.39	−1.80	0.06
F3	1.2	.00	940	741	414	1.8	19	0.4	313	73	23	4.7	0.1	0.62	−1.21	0.30
F4	9.1	.08	912	577	459	1.1	22	0.5	297	72	22	5.0	0.1	1.51	−2.44	2.81
F5	9.3	.77	1396	723	1098	1.1	16	0.4	467	170	29	8.6	1.0	1.52	−1.98	3.59
F6	7.6	.85	1314	619	1260	1.1	15	1.0	399	168	28	8.1	1.0	1.43	−2.14	2.70
F7	6.4	.95	1243	5340	949	1.0	13	1.0	365	155	26	8.3	0.9	1.46	−2.31	2.58
F8			1	4	1	1	1	1	3	1	2	9	0	1	−	2

	5.4	.05	208	97	194	.2	5	.6	50	65	9	.7	.8	.46	2.45	.44	
Atmospheric precipitation																	
Monte				-	1	2	-	3	1	1	0	1	0	0	−	−	-
Rufeno[#]	0.0	.38		.5	.3		.2	.7	.2	.3	.9	.3	.4	5.67	2.15		

Table 3 Stable C-O isotopic composition of the studied fluvial travertines at Bagni San Filippo, Italy.

Sample ID	$\delta^{13}C$ (‰ VPDB)	$\delta^{18}O$ (‰ VPDB)	Type and sampling site
S2-2	6.26	−10.06	Fossil, ca. 20 m downstream of F2
S3-1	6.45	−10.12	Fossil, near F3
S5-1	6.35	−10.61	Modern, ca. 45 m upstream of F5
S5-5	6.35	−10.53	Modern, near F5
S5-3	6.17	−9.96	Modern, ca. 25 m downstream of F5
S6-1	8.06	−10.03	Modern, near F6
S7-1	6.83	−10.11	Fossil, near F7
S7-2	6.83	−9.04	Modern, near F7
S7-3	6.92	−8.90	Modern, near F7
S8-1	7.09	−8.8[illegible]	Modern, near F8
S8-2	6.99	−9.0[illegible]	Fossil, near F8

Table 4 General characteristics of the studied fluvial travertines and possible headsprings (Chiodini et al., 2020), in comparison with those from Aksaz (Turkey) (Özkul et al., 2014), Azuaje (Spain) (Rodríguez-Berriguete et al., 2012; Rodríguez-Berriguete and Alonso-Zarza, 2019), and Ngol (Cameroon) (Bisse et al., 2018; Tchouatcha et al., 2018). Question marks (?) indicate the information not indicated clearly by the previous researchers or deduced from their description.

	Aksaz, Turkey	Azuaje, Spain	Ngol, Cameroon	Bagni San Filippo, Italy
(Nearby) active hot springs (if present; data measured in vents)				
Temperature (°C)	34.9 to 37.6	-	31	23.2 to 48 (mostly near 40)
pH	6.25 to 6.38	-	6.25	6.11 to 7.06
Major ions (mg/L)	Ca^{2+} (346 to 373), Mg^{2+} (87 to 94), HCO_3^- (1326 to 1525)	-	Ca^{2+} (351), Mg^{2+} (165), HCO_3^- (2562)	Ca^{2+} (308 to 702), Mg^{2+} (97 to 181), HCO_3^- (805 to 1714)
Fluvial deposits				
Carbonate facies	Pisoid travertine, crystalline crust, micritic travertine, reed travertine, raft travertine, travertine with fenestral pores	Laminated boundstones, dendrites and shrubs, crystalline facies, rudstone to wackestone rafts, packstone-grainstone ooids, wackestone-packstone-grainstone coated bubbles, wackestone to rudstone oncoids	-	Laminated crystalline crust-boundstone, lime mud, microbial boundstone, phytoherm boundstone, phytoclast rudstone
Mixed clastic-carbonate facies	Lithoclast travertine (with sand matrix)	-	Facies of alternating carbonate layers and argillaceous layers, travertine encrusted detrital facies	Travertine-encrusted breccia, mixed siliciclastic-carbonate sands-gravels
Clastic facies	Conglomerate and sandstone, paleosoil	-	-	sand-gravel sediment
Environments	Waterfall, slope, and pool	Waterfall, pool, and slope	Pool and barrier (waterfall?)	Waterfall, pool, channel, and slope
$\delta^{13}C$-$\delta^{18}O$ (‰ VPBD)	$\delta^{13}C$: 4.3 to 6.3 $\delta^{18}O$: −12.6 to −7.2	$\delta^{13}C$: 4.36 to 10.78 $\delta^{18}O$: −10.41 to −2.08	$\delta^{13}C$: 0.4 to 1.2 (?) $\delta^{18}O$: −8.3 to −5.8 (?)	$\delta^{13}C$: 6.17 to 8.06 $\delta^{18}O$: −10.61 to −8.83
(Paleo-)temperature (°C)	4 to 43 (mainly from 25 to 40)	ca. 40 to 54	-	ca. 25 to 30 (Zone D)
Fluvial erosion	Forming lithoclasts, detrital deposits, and paleosoils on erosional surfaces within travertines; later experienced fluvial incision until today	Existing erosive discontinuities within travertines at several scales; in erosive discontinuity with underlying lava or covering	Existing coated gravels largely formed and transported during flood events	Existing many erosional micro-landforms, (coated) gravels, travertine clasts, and erosive discontinuities

		detrital deposits; later experienced fluvial incision until today		
Scale	Huge build-ups varying from 5 to 24 m thick, hundreds of meters wide and long	Discontinued small build-ups of 1.5 to 4 m thick and up to 10 m long	-	Thin siliciclastic-travertine sequences laterally extending hundreds of meters long
Age (ka BP)	153 to 1.85	2.9 to 3.3	Recently formed and still active	Recently formed and still active
(Paleo-)climate	During the glacial (MIS 6) and interglacial (MIS 3 and MIS 1) periods	Relatively arid, trade wind-dominated climate with torrential rainfalls in winter	Enjoying seasonal fluctuations	Dry summer and wet winter
Local topography	In an large ephemeral stream valley	In a SSW-NNE ravine about 300 m wide	In a stream valley	In a stream valley
References	Özkul et al. (2014)	Rodriguez-Berriguete et al. (2012); Rodriguez-Berriguete and Alonso-Zarza (2019)	Bisse et al. (2018); Tchouatcha et al. (2018)	This study; Chiodini et al. (2020)

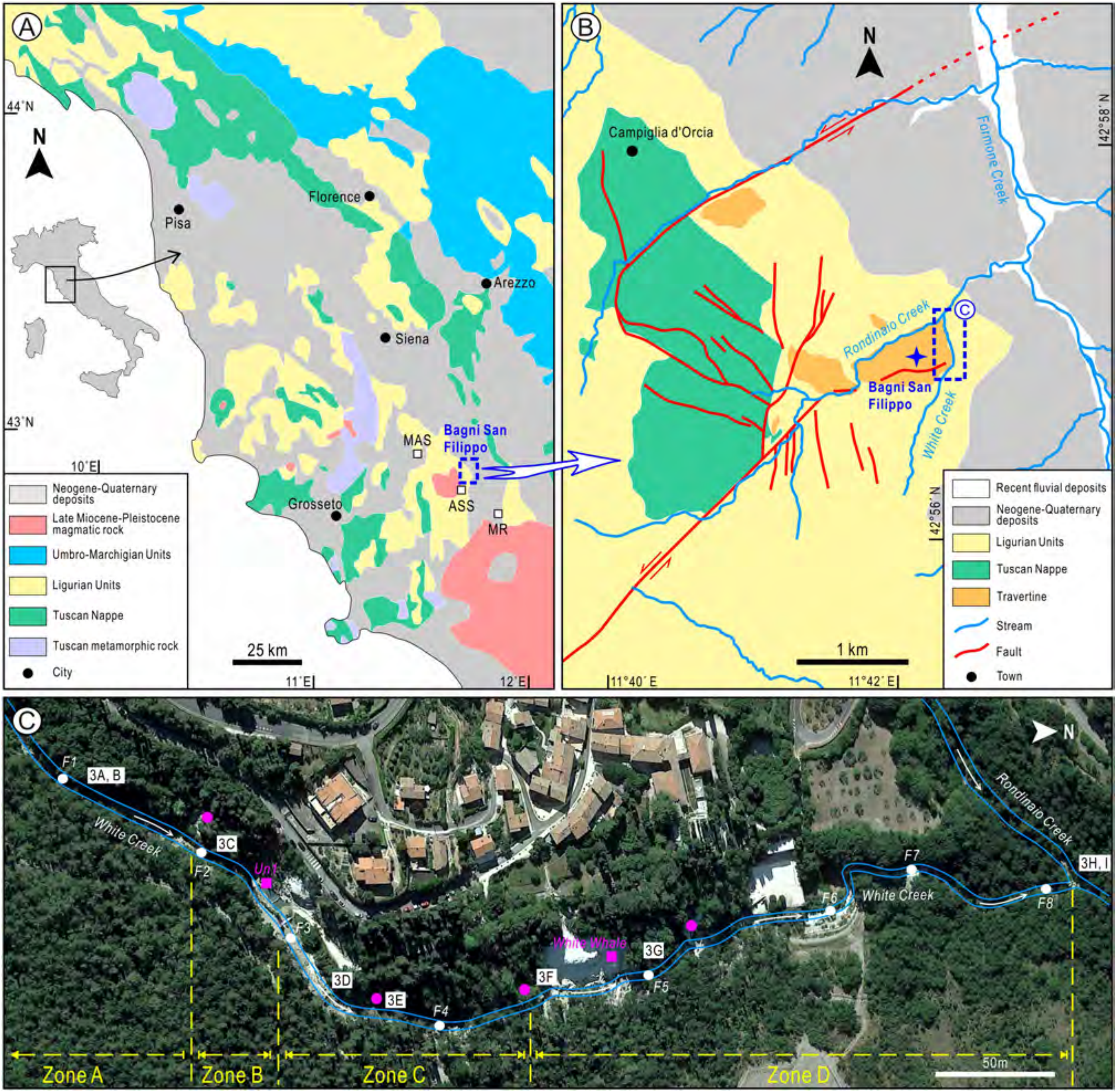
A
44°N
43°N
10°E
11°E
12°E
N
Pisa
Florence
Arezzo
Siena
MAS
Bagni San Filippo
ASS
MR
Grosseto
25 km
Neogene-Quaternary deposits
Late Miocene-Pleistocene magmatic rock
Umbro-Marchigian Units
Ligurian Units
Tuscan Nappe
Tuscan metamorphic rock
City
B
N
Campiglia d'Orcia
Formone Creek
Rondinaio Creek
Bagni San Filippo
White Creek
C
42°58′N
42°56′N
11°40′E
11°42′E
1 km
Recent fluvial deposits
Neogene-Quaternary deposits
Ligurian Units
Tuscan Nappe
Travertine
Stream
Fault
Town
C
N
F1
3A, B
White Creek
3C
F2
Un1
F3
3D
3E
F4
3F
White Whale
3G
F5
F6
White Creek
F7
F8
3H, I
Rondinaio Creek
Zone A
Zone B
Zone C
Zone D
50m

Figure 1

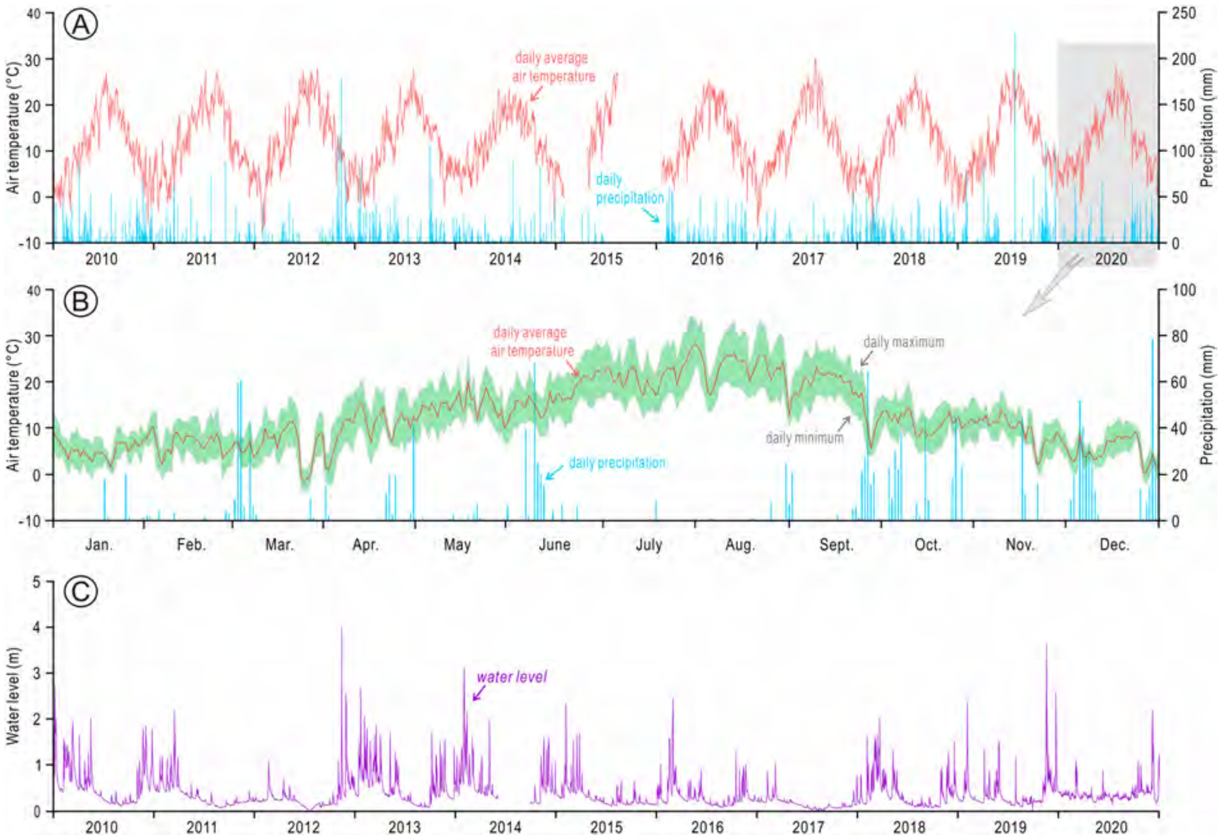

A
B
C
Air temperature (°C)
Precipitation (mm)
daily average air temperature
daily precipitation
daily maximum
daily minimum
Jan.
Feb.
Mar.
Apr.
May
June
July
Aug.
Sept.
Oct.
Nov.
Dec.
Water level (m)
water level
2010
2011
2012
2013
2014
2015
2016
2017
2018
2019
2020

Figure 2

A
2020/12/22
B
2021/06/24
C
D
Un 1
E
F
White Whale
G
White Whale
H
2021/02/04
I
2021/06/24

Figure 3

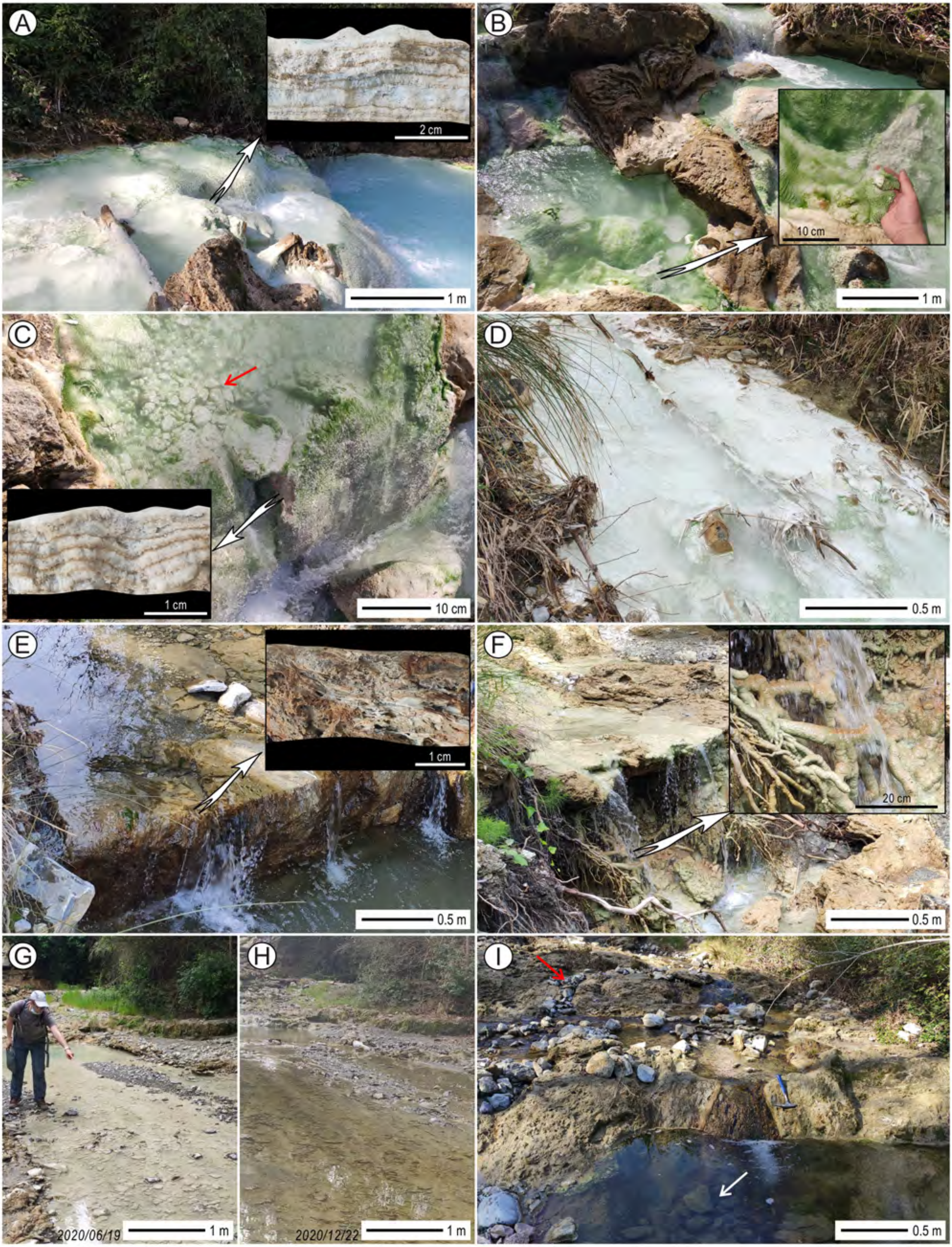
A
2 cm
1 m
B
10 cm
1 m
C
1 cm
10 cm
D
0.5 m
E
1 cm
0.5 m
F
20 cm
0.5 m
G
2020/06/19
1 m
H
2020/12/22
1 m
I
0.5 m

Figure 4

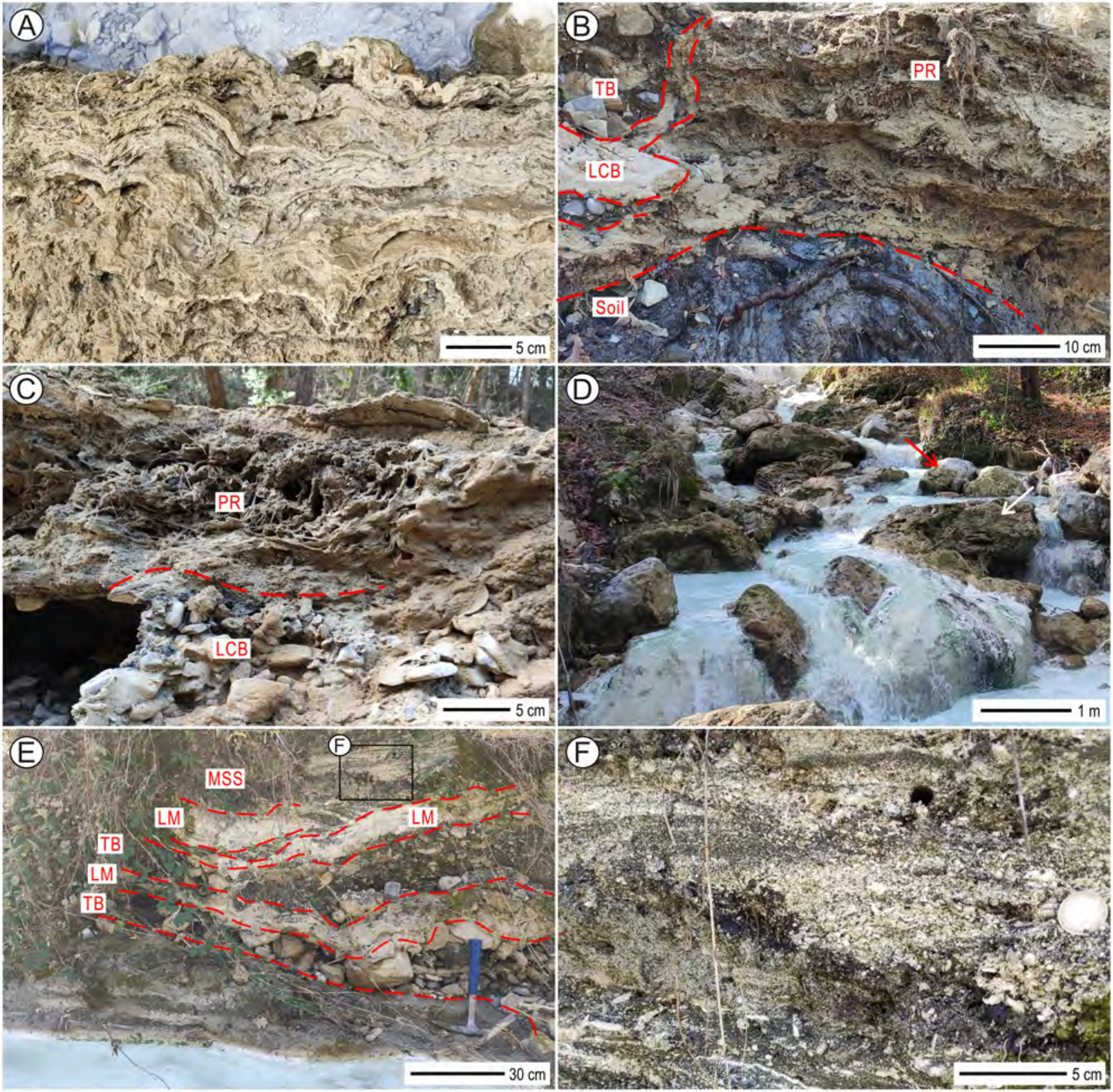
A
5 cm
B
TB
PR
LCB
Soil
10 cm
C
PR
LCB
5 cm
D
1 m
E
F
MSS
LM
LM
TB
LM
TB
30 cm
F
5 cm

Figure 5

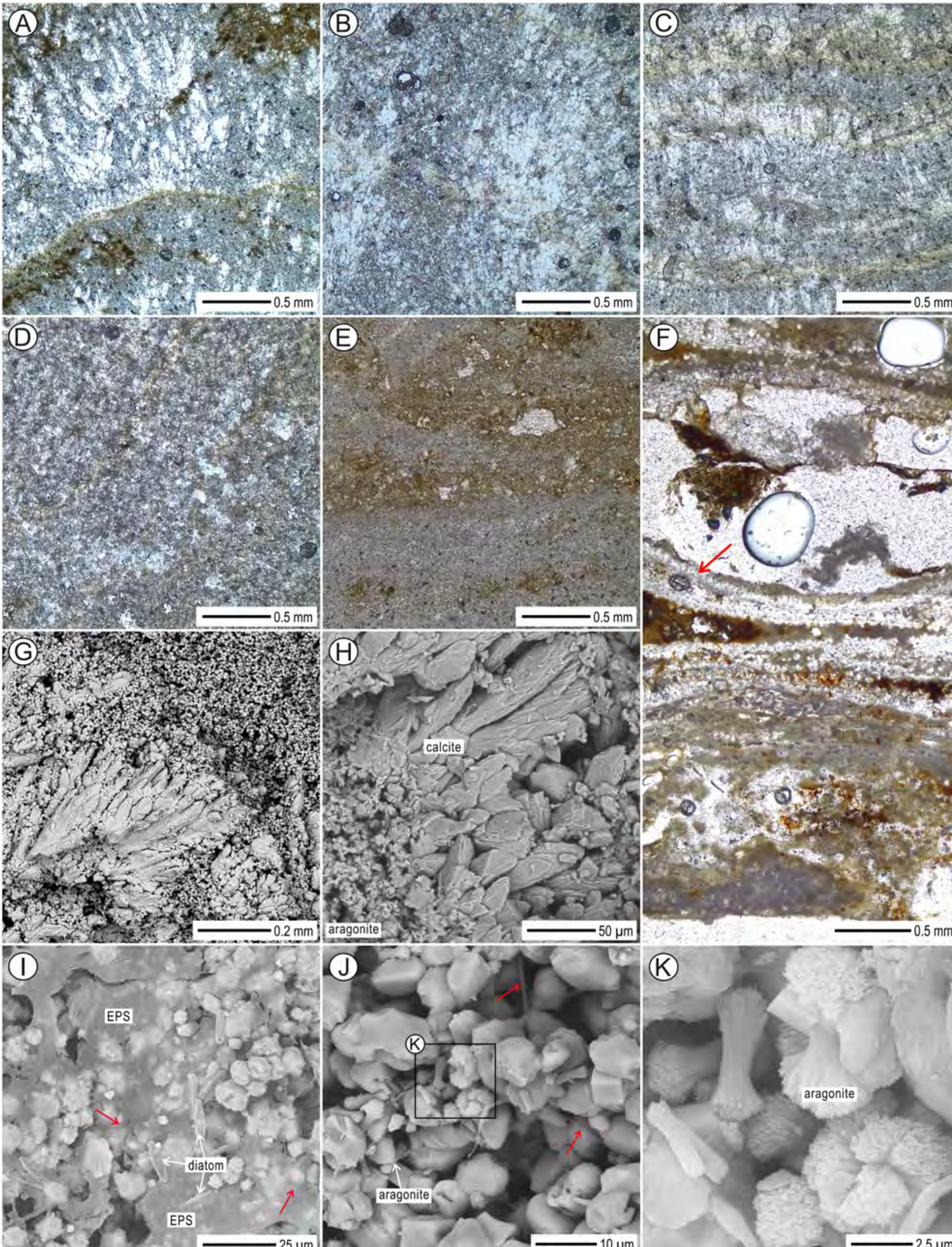
A
0.5 mm
B
0.5 mm
C
0.5 mm
D
0.5 mm
E
0.5 mm
F
0.5 mm
G
0.2 mm
H
calcite
aragonite
50 µm
I
EPS
diatom
EPS
25 µm
J
K
aragonite
10 µm
K
aragonite
2.5 µm

Figure 6

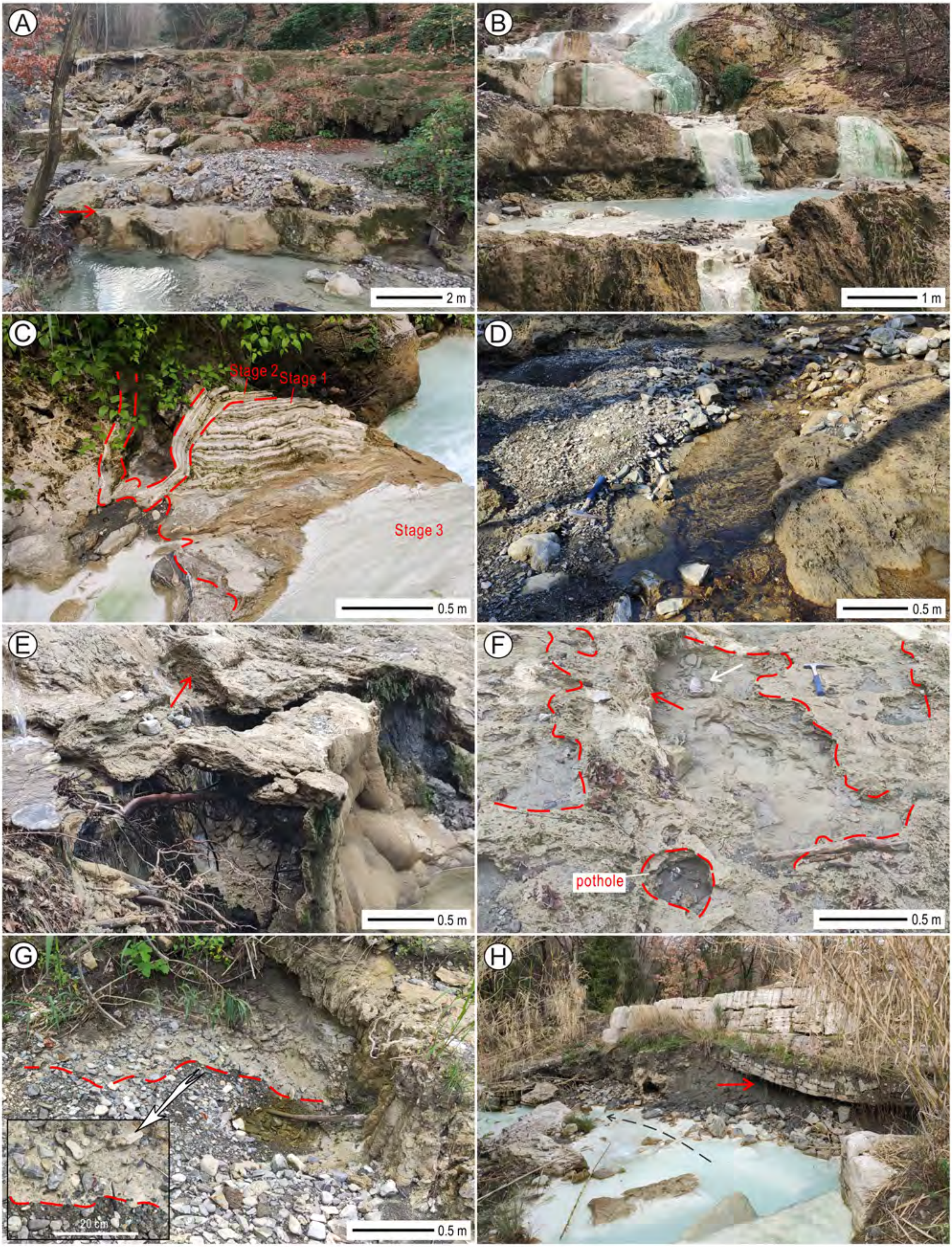
A
2 m
B
1 m
C
Stage 2
Stage 1
Stage 3
0.5 m
D
0.5 m
E
0.5 m
F
pothole
0.5 m
G
20 cm
0.5 m
H

Figure 7

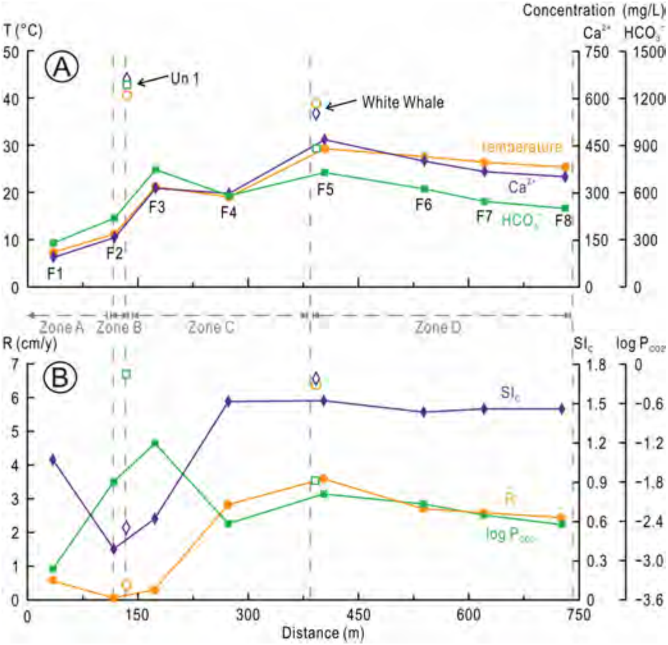

Concentration (mg/L)
T (°C)
Ca²⁺
HCO₃⁻
A
Un 1
White Whale
Temperature
Ca²⁺
HCO₃⁻
F1
F2
F3
F4
F5
F6
F7
F8
Zone A
Zone B
Zone C
Zone D
R (cm/y)
SIc
log PCO2
B
SIc
R
log PCO2
Distance (m)

Figure 8

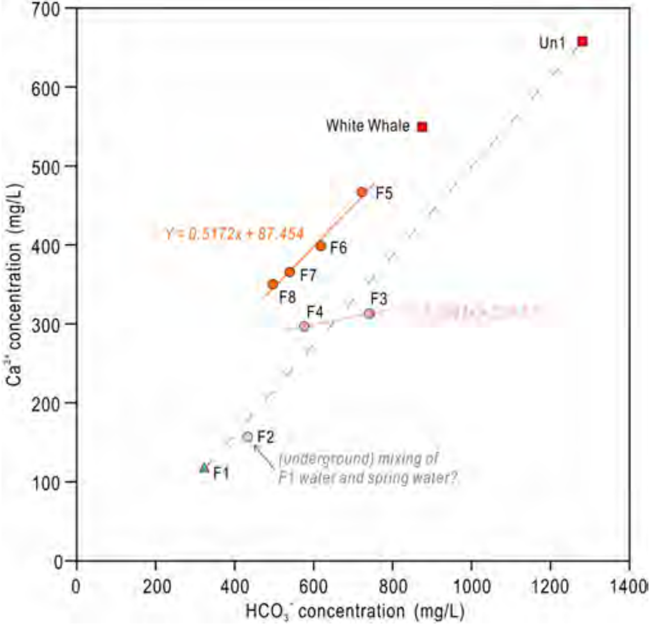

Un1
White Whale
F5
F6
F7
F8
F4
F3
F2
F1
Y = 0.5172x + 87.454
(underground) mixing of
F1 water and spring water?
700
600
500
400
300
200
100
0
0
200
400
600
800
1000
1200
1400
Ca^{2+} concentration (mg/L)
HCO_3^- concentration (mg/L)

Figure 9

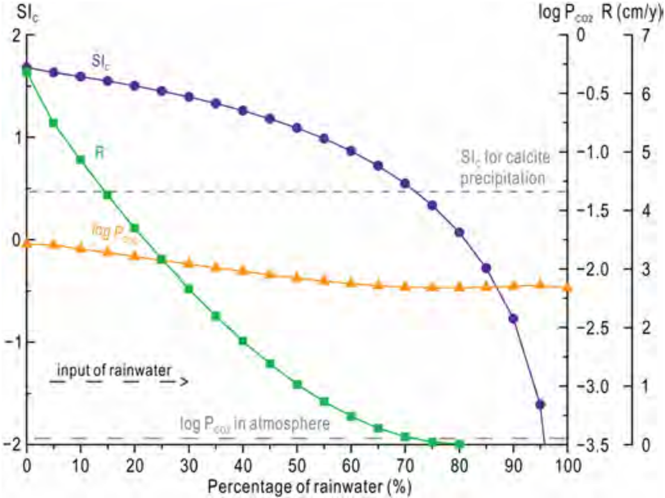

SIc
log PCO2
R (cm/y)
SIc
R
log PCO2
SIc for calcite precipitation
input of rainwater
log PCO2 in atmosphere
Percentage of rainwater (%)

Figure 10

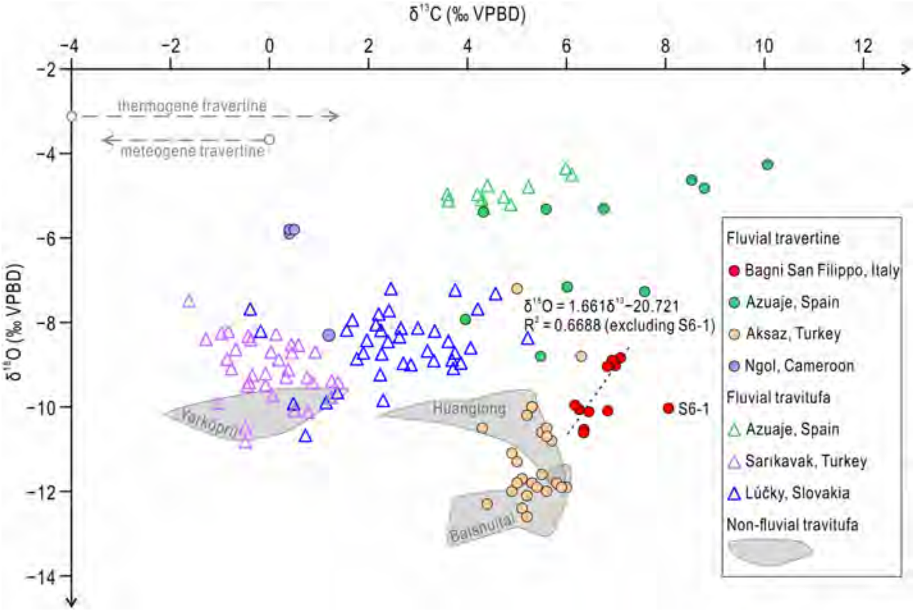
δ13C (‰ VPBD)
-4
-2
0
2
4
6
8
10
12
-2
-4
-6
-8
-10
-12
-14
δ18O (‰ VPBD)
thermogene travertine
meteogene travertine
δ18O = 1.661δ13 −20.721
R2 = 0.6688 (excluding S6-1)
S6-1
Yarkopru
Huanglong
Baishuitai
Fluvial travertine
Bagni San Filippo, Italy
Azuaje, Spain
Aksaz, Turkey
Ngol, Cameroon
Fluvial travitufa
Azuaje, Spain
Sarıkavak, Turkey
Lúčky, Slovakia
Non-fluvial travitufa

Figure 11

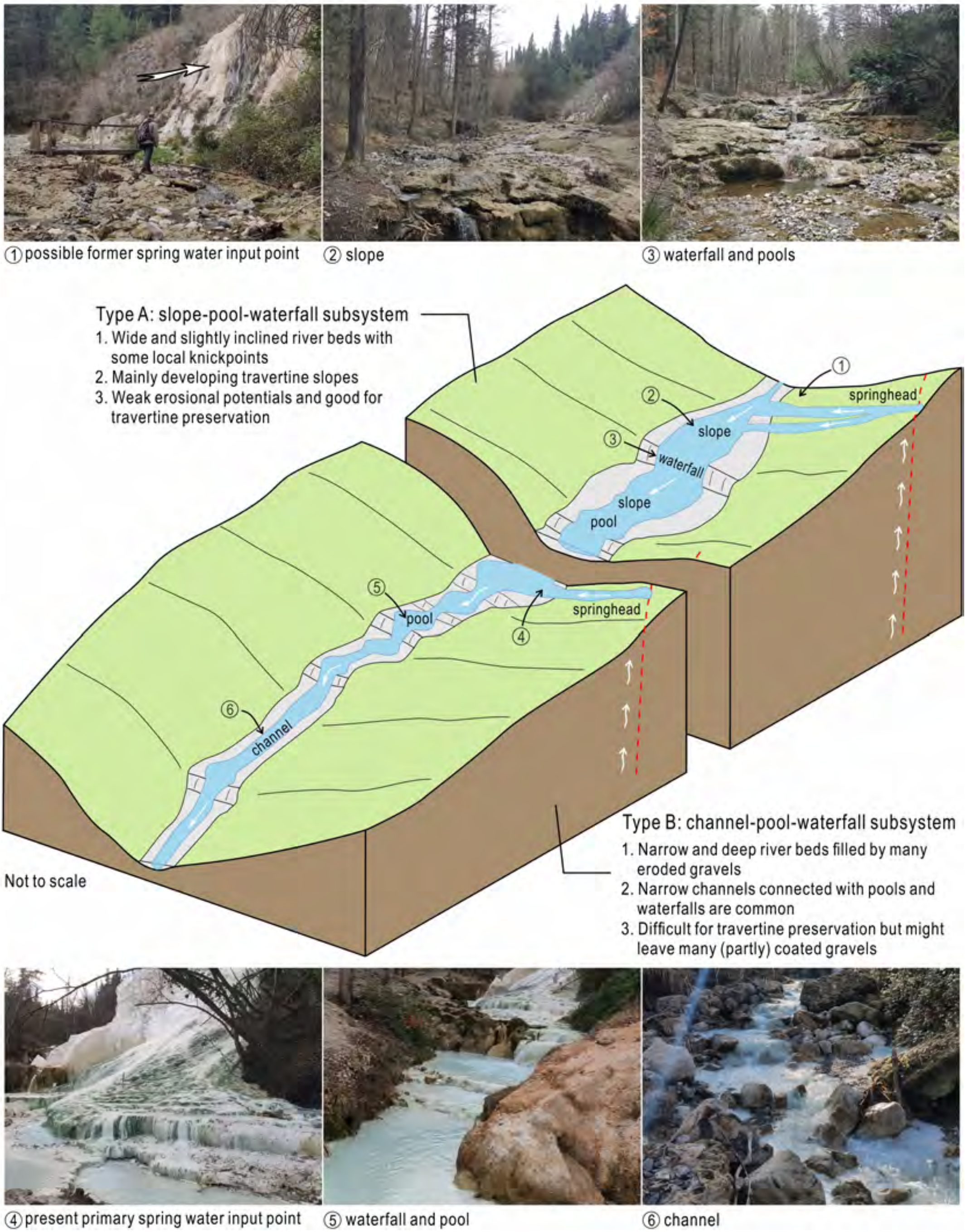

① possible former spring water input point
② slope
③ waterfall and pools
Type A: slope-pool-waterfall subsystem
1. Wide and slightly inclined river beds with some local knickpoints
2. Mainly developing travertine slopes
3. Weak erosional potentials and good for travertine preservation
springhead
slope
waterfall
slope
pool
pool
springhead
channel
Not to scale
Type B: channel-pool-waterfall subsystem
1. Narrow and deep river beds filled by many eroded gravels
2. Narrow channels connected with pools and waterfalls are common
3. Difficult for travertine preservation but might leave many (partly) coated gravels
④ present primary spring water input point
⑤ waterfall and pool
⑥ channel

Figure 12

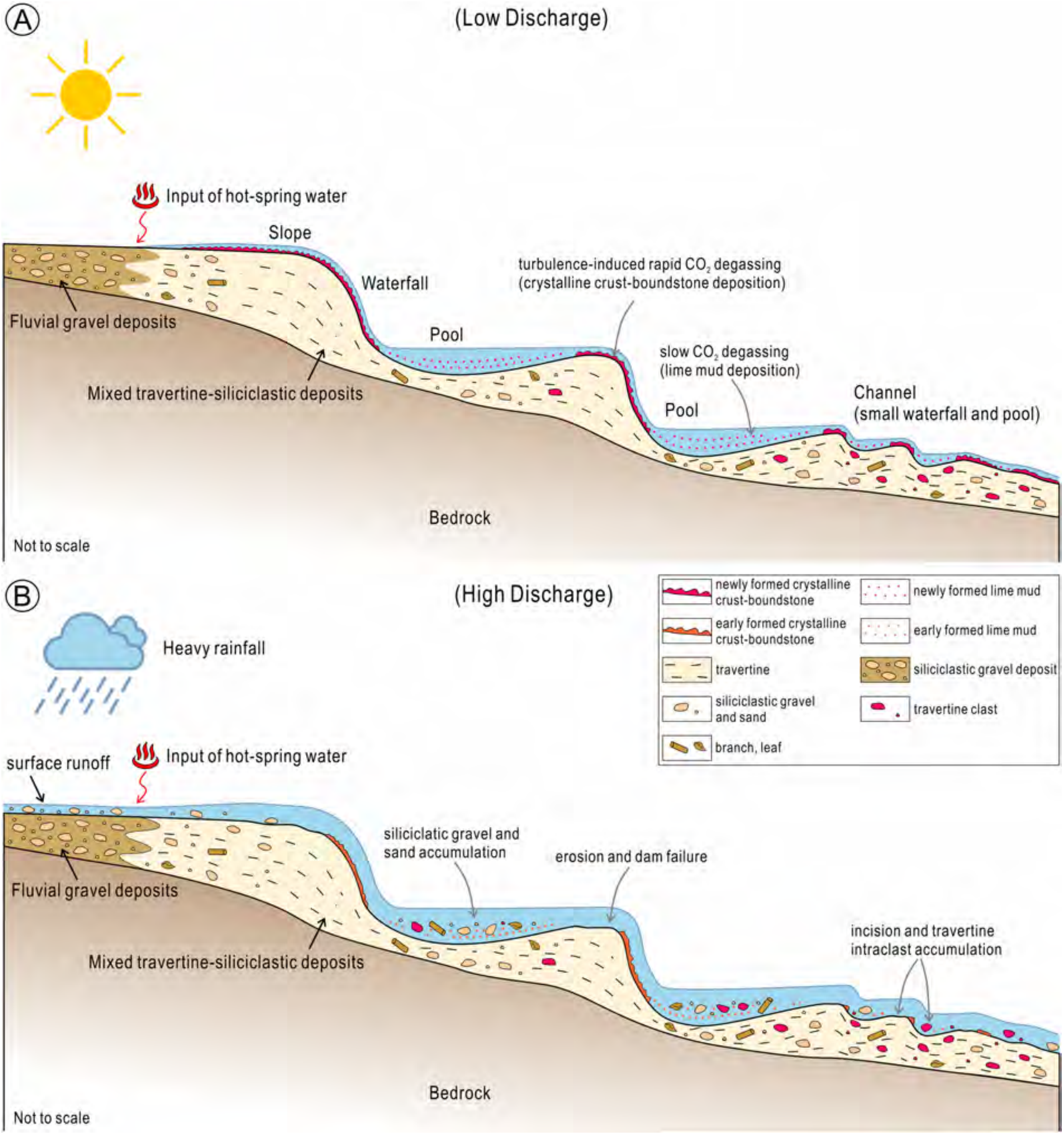

A
(Low Discharge)
Input of hot-spring water
Slope
Waterfall
turbulence-induced rapid CO_2 degassing
(crystalline crust-boundstone deposition)
Pool
Fluvial gravel deposits
slow CO_2 degassing
(lime mud deposition)
Mixed travertine-siliciclastic deposits
Pool
Channel
(small waterfall and pool)
Bedrock
Not to scale
B
(High Discharge)
newly formed crystalline crust-boundstone
newly formed lime mud
early formed crystalline crust-boundstone
early formed lime mud
travertine
siliciclastic gravel deposit
siliciclastic gravel and sand
travertine clast
branch, leaf
Heavy rainfall
surface runoff
Input of hot-spring water
siliciclatic gravel and sand accumulation
erosion and dam failure
Fluvial gravel deposits
Mixed travertine-siliciclastic deposits
incision and travertine intraclast accumulation
Bedrock
Not to scale

Figure 13